Assessing the capability of three different altimetry satellite missions to observe the Northern Current by using a high-resolution model

~~Assessment of the observability of coastal currents in LRM and SAR altimetry observations: a north-western Mediterranean Sea case study~~

Alice Carret[1,2], Florence Birol[1], Claude Estournel[1], Bruno Zakardjian[3]

[1]LEGOS,Université de Toulouse-CNES-CNRS-IRD, OMP, 14 Av. E. Belin, 31400 Toulouse, France

[2]SERCO, Via Sciadonna 24-26, Frascati, Rome, Italy

[3]Université de Toulon, CNRS/INSU, IRD, Mediterranean Institute of Oceanography (MIO), UM 110, 83957 La Garde, France

Correspondence to: Alice Carret : alice.carret@legos.obs-mip.fr

Abstract

Over the last three decades, satellite altimetry has observed Sea Surface Height variations, providing a regular monitoring of the surface ocean circulation. Altimetry measurements have an intrinsic signal-to-noise ratio that ~~strongly~~ limits the space scales of the currents that can be captured~~, and then the geophysical information that can be captured with this instrument~~. However, the recent progress made on both altimetry sensors and data processing~~,~~ allow us to observe smaller geophysical signals, offer~~ings~~ new perspectives i~~n~~n coastal areas where these structures are important.~~terms of research-oriented and operational applications~~. ~~In order to optimize the use of altimetry in coastal areas and thus to estimate which structures are observable by satellite altimetry,. In this paper we present in this paper a methodological study to estimate the signature of altimetry Sea Surface Height of a slope current. We also focus on that helps to better quantifyingquantify the impact of the new technologies and processingthis progress in terms of surface coastal circulation.~~

~~We focus on a case study: the Northern Current, a narrow slope current (less than 60 km wide) located in the North Western Mediterranean Sea. We first use a high resolution numerical model validated with HF radars and underwater glider data to define the general~~

~~characteristics of the Northern Current in terms of surface velocity and sea surface height signature. These characteristics are then compared with corresponding estimates of sea surface height velocity derived from 1-Hz altimetry data sets from three missions: Jason 2 (Ku-band LRM), SARAL (Ka-band LRM) and Sentinel-3A (SAR). The data from all missions were processed with the coastal-specific X-TRACK strategy.~~

In this methodological study we assess the ability of three altimeter missions with three different technologies(~~i.e. JASON2, SARAL/AltiKa, Sentinel-3A) data~~ to capture the Northern Current (North Western Mediterranean Sea) and its variability ~~sea level signature in the coastal (North Western Mediterranean Sea)~~: Jason2 (Ku-band Low Resolution Mode altimeter, launched in 2008), SARAL/AltiKa (Ka-band Low Resolution Mode altimeter, launched in 2013), Sentinel-3A (Synthetic Aperture Radar altimeter, launched in 2016)~~;~~. Therefore, we use a high-resolution regional~~use~~~~using a previously validated high-regional~~ model~~ as a reference~~ as a reference. ~~The impact of the recent progress made on both altimetry sensors and data processing on the observation of the NC is also analyzed.~~

~~Concerning the first step of validation, Wwe~~ We focus along the French coast of Provence where we first show that~~ near Toulon,~~ the model is very close to the observations of High Frequency radars and gliders in terms of surface current estimates~~, providing a very good reference for altimetry data located in this area~~.

In the model, ~~Then the model shows that~~ T~~t~~he Northern Current is observed 15-20 km to the coast on average, with a mean core velocity of 0.39~~44~~ m s^{-1}. Its signature in sea level consists of a drop whose mean value at 6.14°E is 6.9 ~~+/- 2.2~~ cm extending over 20 km~~18 +/- 4~~ km. These variations show a clear seasonal pattern, but high frequency signals are also present most of the time. In comparison,

~~Compared to the model~~~~In~~ In 1-Hz altimetry data, the mean sea level drop associated with the Northern Current is overestimated by 3.6 cm for Jason 2, but significantly less with ~~0.3 cm for~~ SARAL/AltiKa and~~ 1.4 cm for~~ Sentinel-3A: 0.3 cm and 1.4 cm, respectively. In terms of corresponding sea level variability, Jason 2 and SARAL altimetry estimates are larger than the model reference (+1.3 cm and +1 cm, respectively) whereas Sentinel-3A shows closer values (-0.4 cm). When we derive geostrophic surface currents from the satellite sea level variations, w~~W~~ithout any ~~sea level~~ data filtering, in comparison to the model, the standard deviation of~~ altimetry-derived~~ velocity values are also very different from one mission to the other: ~~is~~ 3.7 times too large for Jason-2, but 2.4 and 2.9 times too large for ~~Jason-2,~~ SARAL and Sentinel-3A, respectively. When low-pass filtering altimetry sea level data with different cutoff wavelength, the best agreement between the model and the altimetry distributions of ~~altimetry~~ velocity values~~ies~~ are obtained~~tends to converge towards the model reference~~ with a 6~~5~~0 ~~-~~km, 30 ~~-~~km and 40-50 km cutoff wavelength for Jason-2, SARAL and Sentinel-3A data, respectively. This study shows that using a high resolution model as a reference for altimetry data allows us not only to illustrate how the advances in the performances of altimeters and in the data processing improve the observation of coastal currents but also to quantify the corresponding gain.

1. Introduction

Since the beginning of the 90s, satellite altimetry has enabled many regional circulation studies (e.g. Troupin et al., 2015; Vignudelli et al., 2000 in the NW Mediterranean Sea; Gourdeau et al., 2017 in the Solomon Sea; Liu et al., 2018 in the South China Sea, …). Its main advantages are its long-term and regular temporal coverage and its synoptic character. Large scale structures (>150 km) are well captured with this observational technique which has a crucial role in the knowledge of the circulation at global scale (Fu and Le Traon, 2006). On the contrary, meso-scale and sub-meso-scale processes such as eddies and meanders or narrow coastal currents are historically poorly resolved by altimetry and generally documented by in situ observations or numerical models (e.g. for the NW Mediterranean Sea: Casella et al., 2011; Guihou et al. 2013; Juza et al., 2013; Ourmières et al., 2011; Schroeder et al., 2011). However, during past years, new altimetry techniques have emerged: ~~such as~~ the use of the Ka-band ~~LRM~~ frequency with the SARAL/AltiKa mission (2013+),~~and~~ the adoption of the ~~SAR (~~Synthetic Aperture Radar (SAR) mode with CRYOSAT-2 (2010+), Sentinel-3A,B (2016+, 2018+) and Sentinel-6 (2020+) and a Ka-band Radar Interferometer (KaRIn) with SWOT (launched in December 2022).~~, as well as progress in data treatment,~~ In addition, improvements in re-tracking of radar waveforms and a better characterisation and removal of geophysical corrections such as atmospheric effects or tidal signals have all served to improve the precision of the data retrieved. All these progress have led to a significant~~ly~~ gain in observability of the fine scale ocean structures in general and of the coastal features in particular (Birol et al., 2021; Morrow et al., 2017; Verron et al., 2018).

Despite the progress made, intercomparisons with in situ observations of near-coastal currents have shown that the corresponding altimetry-derived surface velocities are underestimated (Birol et al., 2010; Jebri et al., 2016). In Carret et al. (2019), using long time series of both ADCP (Acoustic Doppler Current Profiler) and glider data as a reference for the Northern Current (NC hereinafter) velocities, we have shown that satellite altimetry data underestimate the amplitude of NC seasonal variations by ~40-45 %. This can be explained by the ageostrophic current component, not captured by altimetry, but also by the effective data resolution, which is limited by the altimeter noise and coastal data processing issues, resulting in near-shore data gaps. This limitation ~~e impact on signal observability varies from one altimeter instrument to another,~~ decreases~~ing~~ with new radar techniques and data processing approaches (Birol et al., 2021; Morrow et al., 2017). Nevertheless, there is ~~still~~ a need to specify more precisely the corresponding improvements in coastal observability ~~related to differences in altimetry technologies (Ka-band, SAR altimetry) and processing techniques~~. It is particularly important ~~n order~~ to optimize the use of altimetry in near-shore areas and to finally define its place among other coastal observation systems~~, it is important to better study the dynamic processes that can be observed and to quantify the associated accuracy~~.

As satellite altimetry measures S~~s~~ea S~~s~~urface H~~h~~eight (SSH or sea level hereinafter), the observability condition is that the processes of interest have a sea level signature and spatio-temporal scales larger than the altimetry resolution. Over the open ocean, the altimetric observability problem is generally studied through a spectral approach (Dufau et al., 2016; Morrow et al., 2017; Vergara et al. 2019). This gives a mean statistical solution over the considered region, but can not be used in the coastal ocean where too short satellite track sections often impede the computation of a spatial spectral analysis. Several studies (Bouffard et al., 2008; Carret et al., 2019; Pascual et al., 2015; Troupin et al., 2015) have used in situ observations to analyze the resolution capability of coastal altimetry data but they came up against the scarcity of independent measurements and their non-colocation in space and/or time.

In this paper, we propose a different strategy based on a high resolution numerical model. Our purpose is to assess the ability of satellite altimetry, using three different technologies, ~~quantitatively analyze~~ to observe~~if~~ a particular coastal dynamical structure ~~can be observed with satellite altimetry new technologies~~. Using a high resolution model may ~~help to~~ overcome the issue of colocation between in situ and altimetry, but given the essential condition that the physical process studied must be correctly represented by the model. Our methodology relies first on ~~After~~ a careful model validation step in the study region. Then, the model is considered as a reference. Our~~our~~ approach will consist in using the model to quantify the SSH signature of an identified physical process along a particular satellite track. In a second time, the~~3~~ model solution will be ~~considered as the reference and~~ compared with the SSH signature captured in the altimetry dataset along the considered tracks and with the resulting geostrophic currents. ~~The observed differences will be analyzed and quantified through different diagnostics.~~

As in Carret et al., (2019), t~~T~~he case study chosen is ~~again~~ the NC in the NorthWestern Mediterranean Sea (NWMed hereinafter). This region is indeed considered as a laboratory area for coastal altimetry studies (Birol et al., 2010; Birol and Delebecque, 2014; Bouffard et al., 2008) because of its small Rossby radius (around 10 km, Grilli and Pinardi, 1998) leading to a wide variety of mesoscale and submesoscale structures. We can also benefit from the variety of in situ data collected from the MOOSE (Mediterranean Ocean Observing System for the Environment, https://www.moose-network.fr, Tintoré et al., 2019) integrated observing system and of the long experience and really good performances previously obtained with the high resolution SYMPHONIE numerical model in the study area (Damien et al., 2017; Estournel et al., 2016; Herrmann et al., 2008).

The NC is a narrow slope current (Fig. 1) formed by the junction of the Eastern (ECC) and Western (WCC) Corsica Currents in the Ligurian Sea (Taupier-Letage and Millot, 1986). It flows cyclonically along the Italian, French and Spanish coasts (Millot, 1987). It has a strong seasonal component with a maximal/minimal transport (maximum of 1.6~~.5-2~~ Sv, Alberola et al., 1995) and increased mesoscale variability in winter/summer (e.g. Crépon et al. 1982; Flexas et al. 2002; Sammari et al. 1995). Its position relative to the coast also varies through the year, from less than 20 km from spring to early November to about 30 km from the coast in November and December (Niewiadomska, 2008; Sammari et al., 1995).~~, as~~ ~~well as its depth~~ Its depth and width also show marked seasonal variations: ~~(~~more than 200 m in winter and 150-200 m during the rest of the year for the depth~~)~~, ~~and width (~~30 km in general with a narrowing in winter~~;~~ ~~(~~Alberola et al., 1995) for the width.

In the past, the NC variability has been intensively studied with in situ observations and models: mesoscale fluctuations at 3-6 days and 10-20 days in Sammari et al. (1995) ; month-long eddies associated in Casella et al. (2011) and, Hu et al. (2011) and day-long eddies in Schaeffer et al. (2011). Birol et al. (2010) have highlighted the contribution of along-track satellite altimetry to study the NC seasonal variability. Since then, other altimetry studies have used such data to investigate the NC circulation as well as the recirculation and associated meanders (case studies in Borrionne et al., 2019; Morrow et al., 2017; Pascual et al., 2015). But none of them have clearly quantified the observation limit (in both space and time), probably for lack of independent sea level and/or current data sets to do so.

Here, we will investigate in details the NC observability issue for three altimetry missions associated to different techniques: Jason 2, with the classical Ku-band Low Resolution Mode (LRM) nadir altimeter, SARAL which uses the Ka-band frequency in LRM and Sentinel-3A (Sentinel-3 hereinafter) with its Synthetic Aperture Radar mode. Section 2 describes the study tools and the model validation step. Section 3 presents the methodology used to quantify the NC sea level signature in the Ligurian Sea and in the area south of Toulon and the results obtained. Section 4 focuses on the NC observation with the three altimetry missions and analyzes the differences obtained between altimetry and the model. Section 5 summarizes and concludes the paper.

2. Data ~~Study tools~~

In this study, in situ (glider), ~~and~~ High frequency (HF) radar and satellite altimetry data are first used to validate a regional numerical simulation ~~(section 2.3)~~. Our study period, strongly constrained by both the in situ data and model simulation availability, goes from 2011 to 2019. The different observing platforms ~~(i.e. HFR, gliders and altimeter missions)~~ and the ~~high-resolution~~ **model are** presented~~described~~ **in sections 2.1 and 2.2, respectively**.~~,~~ ~~while~~ Results of t~~t~~**he model** validation~~assessment methodology versus HF radar and glider data~~ are~~is~~ provided~~detailed~~ **in section 2.3.**

2.1. In situ instruments and satellite altimetry~~Data~~

2.1.a) HF radars

We took advantage of the 2 years of data, from May 2012 to September 2014, provided by the HF Wellen radar (WERA) instruments installed near Toulon as part of the MOOSE network (DOI: 10.17882/56500; Zakardjian and Quentin, 2018). It corresponds to the dataset available at the time of the study. The stations (in orange on Fig. 2a) are located in Cap Sicié and Cap Bénat-Porquerolles in respectively monostatic and bistatic eight-antenna configurations (now upgraded to twelve antenas by site~~, Dumas et al., 2020~~). Their positions enable to monitor the NC upstream the Gulf of Lion~~s~~ (Fig. 2a) and the mesoscale dynamics that occur in this region of cross-shelf exchanges and strong atmospheric forcing (Mistral, Tramontane winds). They operate at 16 MHz with a 50 kHz bandwidth, resulting in a spatial resolution of 3 km, and allow an angular resolution of 2°. The HF radars provide the surface current every hour over a region of 60 x 40 km. Data are then filtered from tides and inertial oscillations ~~to get rid of high-frequency processes not compatible with the hypothesis of geostrophy~~, edited, ~~and~~ averaged daily and finally binned on a regular 2x2 km grid (see Zakardjian and Quentin, 2018 for more details). Note that this data processing removed part of the high-frequency currents, not captured by altimetry that observe only geostrophic currents.

2.1.b) Gliders

In the NWMed, a number of gliders have been deployed since 2005 along different transects, measuring temperature and salinity vertical profiles. We focus on a regular line, from Nice to Calvi where 36 deployments occurred from 2009 to 2016, as part of the MOOSE network. From 2011 to 2017, there are 204 sections ~~(ascending or descending)~~. Data were treated according to Carret et al. (2019) who discarded profiles being too short or deviating too much from an average Nice-Calvi trajectory. It results in temperature and salinity data down to 500m (depth reached by all gliders), gridded with a 4 km horizontal bin size along the mean trajectory considered as a reference track. The temperature and salinity data are then filtered using a 15 km cutoff wavelength. The geostrophic velocity component perpendicular to the reference track is then derived using the thermal wind equation referenced to 500 m (see Carret et al., 2019 for further details).

2.1.c) Satellite altimetry

Jason 2 was launched in June 2008 and was in the same orbit up to October 2016. It is based on the~~a~~ conventional ~~Low Resolution Mode (~~LRM~~)~~ altimeter operating in the Ku-band and has a 10-day repetition cycle. SARAL, launched in February 2013~~ moved to a drifting orbit in July 2016~~, provides~~ing~~ a shorter data time series (~3 years) because it moved to a drifting orbit in July 2016. It has a 35-day repeat observation cycle.~~. However, with~~ I~~i~~ts Ka-band LRM altimeter ~~operating in the Ka-band (~~(called AltiKa) has a smaller footprint than the Ku-band instruments: ~4 km radius against 5-7 km.~~,~~ The corresponding~~it has a~~ lower data noise allows to~~and is expected to~~ capture smaller spatial scales than Jason 2 (Verron et al., 2018). The Ka-band is also less affected when crossing the ionosphere and provides a better estimation of the surface roughness. Sentinel-3 was launched in February 2016. With its Synthetic Aperture Radar (SAR) altimeter, its footprint is even more~~further~~ reduced in the along-track direction, compared to LRM altimeters~~ SARAL~~: ~0.3 km. It~~Sentinel-3~~ has a 27-day repeat observation cycle. .

Figures 2b,c,d indicate the satellite tracks of each mission in the NWMed, defining the spatial coverage of the corresponding nadir altimetry observations. Note that the spatial resolution of nadir 1-Hz altimetry data is in the range 5-8 km along the track (Table 1) but that the inter-track distance varies from 230 km for Jason 2 to 76 km for Sentinel-3 and 58 km for SARAL. For each mission, the tracks used in this study are indicated in bold in Fig. 2b,c,d. They correspond to the tracks closest to HF radars data (see below for explanation): the Sentinel-3 track 472 and the SARAL track 302 pass over the HF radars region with a different angle, whereas the Jason 2 track 222 is located a bit further to the east, at about 60 km. As along-track ~~satellite~~ altimetry data allows to derive only the across track currents, through the geostrophic assumption, the angle of the track~~s~~ with respect to the current vein has a major~~n~~ impact on the current capture~~ of currents~~: the less~~ more the current is~~ perpendicular ~~to~~ the track, the less realistic~~stronger~~ the~~its~~ amplitude~~ will be~~. Concerning SAR altimeters the observation of a current perpendicular to the track will benefit from the corresponding increase in resolution. Table 1 summarizes the characteristics of each altimetry dataset.

For all missions, we use the X-TRACK, a~~A~~long-track Sea Level Anomalies (Version 1.02 - 2017 – DOI: 10.6096/CTOH_X-TRACK_2017_02) ~~X-TRACK~~ regional product processed with a coastal oriented strategy described in Birol et al. (2017). (DOI: 10.6096/CTOH_X-TRACK_2017_02) thatIt provides 1-Hz Sea Level Anomaly (SLA) time series homogeneously processed and regularly spaced (Table 1, along-track resolution) along the different satellite tracks. The processing is the same for all missions, except that the dual-frequency of Jason 2 and Sentinel-3 altimeters allows to compute the ionosphere correction whereas a model is required for SARAL. This correction being associated with long wavelengths, it should not impact the results obtained in this study.

To obtain the Absolute Dynamic Topography (ADT), the X-TRACK SLA data are added to From SLA data, the across-track geostrophic current (*u*) can be inferred through the geostrophic equation (Eq. 1) after adding a regional Mean Dynamic Topography (SMDT-MED-2014, developed by Rio et al., 2014MDT, Rio et al., 2014)-. Then the absolute across-track geostrophic velocity (u) is derived from the geostrophic equation (Eq 1).

$$u = \frac{-g}{f} \frac{\Delta(SLA+MDT)}{\Delta x} \qquad (1)$$

where g is the gravitational constant, f the Coriolis parameter and Δx the distance between the 1-Hz altimetry points. Before adding the MDT and computing current estimates, the SLA may be filtered in the along track direction in order to remove the remaining altimetry noise. To investigate the data noise issue, both, unfiltered and filtered 1Hz SLA data have been considered for the computation of geostrophic velocities in sections 4.1 and 4.2, respectively. In this study the filtering is applied in Section 4.2 but not in Section 4.1. The filtering is done with a low-pass Loess filter using different cut-off wavelengths (see Section 4.2) .

2.2. Model

We rely here on the SYMPHONIE primitive equation model which has been widely used in the study area at the nearshore (Michaud et al., 2012), coastal (Estournel et al., 2003; Mikolajczak et al., 2020; Petrenko et al., 2008) and regional (Estournel et al., 2016) scales. Validation studiess **of** SYMPHONIE currents over the Gulf of Lion have been carried out by comparison with various instruments on different hydrological structures and meteorological situations: VHF radars on the Rhone plume (Estournel et al., 2001), hull-mounted ADCP (Estournel et al., 2003) in prevailing northerly winds, fixed ADCP (Mikolajczak et al., 2020), and glider drift (Gentil et al., 2022) during easterly storms.

SYMPHONIE is described in Marsaleix et al. (2008, 2006), Damien et al. (2017), with turbulence closure and convection parameterization detailed in Estournel et al. (2016). The configuration used in this study covers the whole Mediterranean basin, the Marmara Sea and extends westward up to 8°W in the Gulf of Cadiz as ~~; it is~~ described in Estournel et al. (2021). The horizontal resolution is minimum (2 km) in the northwestern Mediterranean (except for a local narrowing at the Gibraltar strait). A VQS (V~~v~~anishing Q~~q~~uasi-S~~s~~igma) vertical coordinate (Estournel et al., 2021) with 50 levels is used. The model is initialized and forced at its open boundaries with analysis produced by the operational oceanography center MERCATOR OCEAN International, (MOI, Lellouche et al., 2013). As stratification is crucial for mesoscale characteristics, it has been debiased from observations collected over the whole basin as in Estournel et al. (2016) while preserving the first hundred meters which benefits optimally from the data assimilation performed at MOI. At the air/sea interface the hourly forecasts of ECMWF(European Centre for Medium-Range Weather Forecasts) based on the high resolution 10-day forecast (HRES product) ~~+ citation~~ at the horizontal resolution of 0.125° are used to calculate heat and momentum fluxes through bulk formulae.

The model simulation covers the period from 18 May 2011 to 31 March 2017 and provides 4-day averaged fields. ~~Daily outputs are also available during the period of HF radars availability and will be used in the validation exercise (section 2.3).~~

2.3. SYMPHONIE model assessment ~~Simulation validation~~

~~The first step of this study is to validate the model simulation in terms of surface current which is here the variable of interest. The currents deduced from the gliders and HF radars are compared to their equivalent in the simulation: geostrophic ones for the glider, total currents for the radars. The representation of the NC is compared using statistics (time-average and standard deviation) and time-space diagrams (Hovmuller diagrams).~~ The model performance to represent the NC velocity field ~~signal~~ in the study area ~~in the velocity field~~ is assessed quantitatively in terms of statistics(~~i.e.~~ time-average and standard deviation) and ~~the NC variability is evaluated~~ qualitatively in terms of complete range of variability (Hovmöller diagrams).

For the comparison with the HF radars, we consider the zonal current component from May 2012 to September 2014 along a section located at 6.14°E, just south of Toulon (Fig. 2a). The model equivalent ~~for the total currents~~ is extracted~~projected~~ along this section with the same spatial and temporal resolution~~s~~ as the HF radars. Daily outputs for the model during the HF radars period are used. Note that, due to the coast configuration, in this area, the NC which follows the 1000-2000m isobaths is mainly westward, i.e. with a dominant zonal component most of the time (with the exception of short living, 3-6 days, meanders or wind-induced instabilities). Figure 3a shows the time-average and standard deviation of the zonal velocity as a function of latitude along this section. At this longitude, the NC flows westward and corresponds then to the negative values observed north of 42.7°N. In terms of statistics, there is an excellent agreement between the HF radars and the simulation. On average, the NC position and current amplitude are almost identical in both fields. The mean ~~maximum~~ NC core velocity ~~amplitude~~ (called Vmax hereinafter) is -0.44 ± 0.16 m s^{-1} for the simulation and -0.43 ± 0.19 m s^{-1} for the HF radars. This velocity value, identified as the NC core, is located at 42.85°N for both simulation and observations. We define the width of the NC as the length of the section around its core where the absolute velocity is larger than |Vmax|/2. On average, it is 18 ± 5.9 km for the simulation and 18 ± 6.1 km for the observations. All these figures are summarized in Table 2. The main difference along the section is that between the NC and the coast (to the north), ~~where~~ the velocity variability is slightly greater for the HF radars than for the simulation.

In order to investigate the representation of the NC variability in the simulation in more detail, Fig. 3c represents the ~~time-space diagrams~~Hovmöller diagrams of the zonal velocity along 6.14°E for both the HF radars and the simulation and the differences between both fields. We observe an overall good agreement between the observations and the simulation, both estimates showing the same seasonal variability, i.e. larger velocities in winter and spring and a summer slow down, and a similar high frequency variability that may instantiate the wind-induced (Ekman current) and mesoscale (meanders and eddies) variability of the circulation. The differences between the currents' estimates are generally low and higher values (order of a few tens of cm s^{-1}) can be largely explained given the fact that short-living structures may not strictly coincide in time and space in the model and observations.

The same diagnostics have been computed for the simulation and the glider data along the Nice-Calvi section, located further east (Fig. 3b,d) but in this case with the geostrophic current component normal to the section (Table 2). Here, t~~T~~o get as close as possible to the data, ~~with the model~~ we used the vertical temperature and salinity model profiles~~fields~~ extracted~~projected~~ along the Nice-Calvi section and ~~along the water column before~~ then computed~~ting~~ the geostrophic velocities with the same method aes for~~according to~~ the gliders ~~method~~. We also observe a good agreement between the simulation and the gliders but with higher ~~more~~ differences than what was obtained with the HF radars, especially in terms of current variability. We obtain Vmax values of -0.23 ± 0.12 m s^{-1} for the model and -0.25 ± 0.13 m s^{-1} for the gliders. Near the coast the differences between the observed and simulated mean currents can reach 0.1 m s^{-1}. The NC core is located at 43.51°N for the simulation and at 43.52°N for the observations. The NC is thus well located in relation to the coast in the simulation, but narrower (24 ± 6.6 km), compared to the observations (30 ± 9.6 km). Concerning the Hovmöller diagrams ~~time-space diagrams~~, the instantaneous differences in velocity between the observations and the simulation can reach 0.5 m s^{-1}. They are associated with a misplaced current in time in the model rather than with incorrect current maxima ~~values~~. The irregular temporal sampling of the gliders also contributes to these larger qualitative model-data differences, compared to the HF radars results. Indeed, a deeper analysis shows that the same features may occur in the simulation and in the observations, but shifted by one or two days (not shown). In such cases, they are captured ~~Thus they are represented in the~~ by daily HF radar equivalent ~~s Hovmöller diagram~~ but may correspond to gaps in the irregular glider equivalent~~diagram~~.

~~Finally, we have used all the observations available (glider, HF radars and altimetry) in order to have a general view of the model ability to represent the regional circulation in our study area (Fig. 4). For the sake of clarity, we chose to represent for SARAL only the tracks closest to in situ observations in order to not overload the figure. We compute the time-average and the standard deviation of surface current perpendicular to the tracks derived from all observations and from the simulation collocated in space and time with the observations (Fig. 4). These statistics are computed over the common period of data availability (if we consider only SARAL and Jason-2 in terms of altimetry missions): from March 2013 to October 2014. Both a regional view of the NW Mediterranean Sea and a zoomed-in view of the northern Ligurian Sea are provided. Note that the observation component of these diagnostics (top panels) have already been shown in Carret et al. (2019) to analyze how the NC is captured by the different types of instruments while the focus here is on the simulation quality. In Fig. 4a and c, the NC corresponds to the negative velocity values (westward flow) represented in blue along the French and northern Spanish continental slope. As already indicated in Carret et al. (2019), the continuity of the circulation emerges when putting together the different instruments which show a very good consistency in terms of mean current. The model also shows this continuity with almost identical current values: around -0.19 m s^{-1} south of Nice against -0.24 m s^{-1} for the gliders and around -0.42 m s^{-1} south of Toulon against -0.41 m s^{-1} for the HF radars. The standard deviation of the current is larger along the NC. It is captured by all types of observations but with differences from one instrument to the other (see Carret et al., 2019 for analysis). These differences due to the sampling bias and the spatial variability are also observed in the simulated field, although the corresponding standard deviations are~~ lower ~~weaker. At the HF radars location, the NC variability results in standard deviation values of 0.24 m s^{-1} for the observations and 0.14 m s^{-1} for the simulation, which is coherent with what is observed on Fig. 3. The variability is less important for altimetry data which~~ do not ~~don't get as close to the coast as in situ observations and measure a different geophysical content than the observations. Carret et al. (2019) showed that these differences mainly come~~

~~from the temporal resolution and the number of data samples.~~

All these results show that the simulation has excellent skills in terms of circulation, ~~as well at the regional scale all along the NC paths than~~ especially at the local one in the vicinity of the HF radars and glider covered areas.

3. Signature of the NC on sea level

The good results obtained above in the Ligurian Sea and ~~in the area~~ s~~S~~outh of Toulon in terms of model-data comparison allow us to use the simulation as a reference for altimetry data analysis. It is first used to quantify the NC sea level signature before analyzing how it is captured by altimetry data (section 4). We first describe how we quantify this signature using the ~~over the area covered by the~~ HF radar zonal section~~s~~ described in Section 2 ~~observations~~.

In the simulation, we first extracted the sea level profile~~s~~ for each date along the section located at 6.14°E (see Fig. 2a). The corresponding cross-transect surface geostrophic current component is then calculated using Eq. 1, as for classical altimetry estimates.

For each SSH profile, we use three diagnostics to characterize the NC sea level signature. First, the location of the NC core, corresponding to the maximum velocity in absolute value, is spotted on the cross-shore current profile (expressed as a distance to the coast). Then, the drop in SSH (called *diff*) is computed over the region delimited by velocity values higher than half of the NC core velocity (Eq. 2, Niewiadomska et al., 2008).

$$diff = max\left(SSH_{|u| \geq \frac{|u|max}{2}}\right) - min\left(SSH_{|u| \geq \frac{|u|max}{2}}\right) \quad (2)$$

Finally the width (*dx*) of this region, considered as ~~defining~~ the NC width, is derived as the distance between the two half NC core velocities (Niewiadomska, 2008). This criterion offers the advantage of not being impacted by seasonal differences in the NC amplitude.

Figure 4~~5~~ illustrates the methodology described above for the model SSH and corresponding zonal current profiles along the 6.14°E transect and averaged over the HF radars period. The profiles are represented as a function of the distance to the coast. On Fig. 4~~5~~a, the dashed vertical lines delimit the NC width. They are transposed on Fig. 4~~5~~b in order to derive the corresponding SSH drop (*diff* value).

We observe that, on average, the SSH decreases from 8 km to 28 km to the coast, i.e. the distance *dx*. This corresponds to the NC associated with negative zonal velocity values. Still on average, the NC core velocity is -0.39 m s^{-1} and is at about 18 km from the coast. It corresponds to a drop in sea level of 6.9 cm over 20 km. These values are considered as the mean sea level signature of the NC in the area considered.

The time series of the three diagnostics defined above along the 6.14°E transect are represented in Fig. 4~~5~~c. The SSH drop associated with the NC varies between 2 cm and 15 cm, with a clear seasonal tendency. Greater values are generally observed in winter and smaller values in summer. The NC core position varies between 10 and 30 km from the coast (30 km in Alberola et al., 1995) with a slight seasonal variation. It is a little closer to the coast in autumn than in winter, in agreement with Niewiadomska et al. (2008) and Sammari et al. (1995), even if these previous studies were not in the Toulon area. The NC width spreads over 10 to 25 km, depending on the season (it is the widest in January and July and the narrowest in March and April). Previous studies (Alberola et al., 1995) show a NC narrower and faster in winter, it may depend on the NC orientation in relation to the section: a NC not purely perpendicular may artificially increase the current width. In the different diagnostics, the high frequency variability is also important, with some strong peaks. This may be due to intense wind events which induce meanders or eddies in the HF radars area (Guihou et al., 2013). Note that in August 2013, the NC core shifted until 50 km from the coast, associated with a large width and strong SSH drops (Fig. 5c). It is also visible on Fig. 3 for both the simulation and the HF radars. We investigated what happened for the corresponding dates, from 25 to 28 August 2013, in both simulated and observed surface currents (not shown). We observed that the NC is then totally deviated to the south and is cut in two parts, with a recirculation loop that comes from the south-west and blocks the NC flow. The good agreement between the model and the HF radars during~~concerning~~ this extraordinary event is a~~nother~~ proof of the model reliability to reproduce the high frequency variability of the NC~~shown in section 2.3~~.

If we consider the global Root Mean Square (RMS) ~~mean~~ error level for the altimetry missions which is 2.23/1.66/1.12 cm for Jason-2/SARAL/S3A, respectively (Vergara et al., 2019), the NC signature on SSH corresponds to greater values and thus might be observable. But its width is generally below the scales resolved. Indeed Jason satellites can capture offshore dynamical signals down to ~70 km wavelength and SARAL/AltiKa and Sentinel-3 down to 35-50 km (Raynal et al., 2017). We also know that the observation of near-shore SSH estimates is a technical challenge for altimetry (Vignudelli et al., 2011). In the next section, using the model as the reference, we analyze which part of the NC SSH and current signals are really sampled by altimetry data.

~~In terms of SSH drop, the NC signature is then generally above the global~~ RMS ~~rms mean error level for the altimetry missions considered here (from Vergara et al., 2019: 2.23/1.66/1.12 cm for Jason-2/SARAL/S3A, respectively). But its width is generally below~~

the scales resolved (from Raynal et al. (2017), Jason satellites can capture offshore dynamical signals down to ~70 km wavelength, SARAL/AltiKa and Sentinel - 3 down to 35 - 50 km). We also know that the observation of near-shore SSH estimates is a technical challenge for altimetry (Vignudelli et al., 2011). In the next section, using the model as the reference, we analyze which part of the NC SSH and current signals are really sampled by altimetry data.

4. Observability of the NC in altimetry data: from Jason-2 to Sentinel-3

In this section, we first analyze the general characteristics of the SSH and surface (cross-section) velocity profiles observed along the selected tracks (see section 2.1 and Fig. 2) for both altimetry data and the model reference (section 4.1). The altimetry data noise issue is then investigated in section 4.2.

In this section a quantitative assessment of the NC sea level signature (in terms of SSH drop, NC width and distance to the coast) is performed for the three altimeter missions and the reference model. We consider both unfiltered (section 4.1) and filtered (section 4.2) 1 Hz SLA data for the computation of geostrophic velocities in sections 4.1 and 4.2, respectively, to analyze the importance of applying spatial filters to altimeter data in order to obtain a better agreement with the model.

4.1 SSH and current statistics

We compute the temporal mean and standard deviation of the individual SSH and corresponding cross-track velocity profiles (using Eq. 1the geostrophic equation) observed along Jason 2 track 222, SARAL track 302 and Sentinel-3 track 472 (Fig. 56). The corresponding model estimates at the dates closest to altimetry are also calculated and shown in the same figures. The model fields are interpolated at the 1-Hz altimetry points along each track (i.e. every 6-7 km depending on the altimetry mission). Note that here, no spatial filtering is applied on altimetry data, neither on the SSH nor before computing the geostrophic velocities, because we want to analyze the resolution capability of raw sea level data. The geostrophic current derived from the MDT is also shown on Fig. 5b,d,f to estimate its contribution in the total geostrophic current. For Jason-2 and SARAL missions, periods were selected based on the joint availability of both observations and model outcomes (see in Table 32). For Sentinel-3, the matching period was very short, so thus the full data availability periods for observations and model were considered. For Jason-2 and SARAL, the time periods considered are the common periods between observations and the model simulation: 27/05/2011-01/10/2016 for Jason-2 and 24/03/2013 to 13/03/2016 for SARAL. For Sentinel-3, the common period of model and data availability is very short (18/06/2016 to 15/03/2017). We then chose to use the total period of Sentinel-3 data availability (18/06/2016 to 14/03/2019) and the period 21/06/2014 to 15/03/2017 for the model (same length but different years). To estimate the impact of this choice on the results, we performed a sensitivity analysis by computing the mean current and the mean SSH of the model (same diagnostics than those on Fig. 56) over different 3-year time periods: over 10/06/2011 - 31/03/2014, 22/06/2012 - 17/03/2015, 08/06/2013 - 29/03/2016. The results are very similar (not shown), which indicates that in this area the interannual variability does not have a strong imprint on our results.

The three diagnostics defined in section 3 are considered for each mission - the SSH drop associated with the NC, the NC width and the distance to the coast of the NC core - and extended up to 120 km of the coast. The statistics are computed with 195, 32, 36 samples for Jason-2, SARAL and Sentinel-3, respectively (see Table 1).

We first focus on Jason-2 results. In Fig. 56a, we observe that on average, the raw altimetry SSH profile agrees fairly well with the model above 20 km from the coast; below this distance, the two curves diverge with a steeper slope for Jason 2. In this area, the SSH increase corresponding to the external edge of the NC starts at 60 km to the coast, i.e. further from the coast than for the 6.14°E transect (located to the west). The 1-Hz altimetry SSH data stops at 8 km from the coast. SSH standard deviations from altimetry are slightly greater (between 0.8 and 1.6 cm) than from the model, except at the nearest point to the coast where the difference reaches 2.2 cm. Figure 56b shows the corresponding mean cross-track velocity profiles. Jason-2 solution is noisier than the model one and the one derived from the MDT. Here again, above 20 km from the coast the two mean curves of the model and altimetry agree well but when approaching the coast, the steeper slope observed in Jason-2 SSH results in too high near-coastal velocity values and then a larger NC, in comparison to the model. The standard deviation of Jason 2 velocities is about three times higher than for the model (0.34 m s^{-1} against 0.092 m s^{-1}).We also observe that the current variability tends to decrease near the coast in the model, whereas it increases in the observations, likely due to nearshore increased altimetry noise.This was also shown in section 2.3 when the model was compared to the HF radars. As we focus on the mean SSH over a long period the results are close to the MDT along the section. However the contribution of the SLA is given by the variability indicated by the error bars. We can also note that the current obtained from the average of individual current profiles compared to the one derived from the MDT is quite different which means that the SLA variability plays a key role in deriving the currents.

Figure 56c,d shows the same analysis for SARAL. It should be kept in mind that the 35-day cycle of SARAL and its shorter lifetime lead to a significantly smaller number of samples to compute the statistics compared to Jason-2. Figure 56c shows the SSH profiles. Here, 1-Hz altimetry data stops at 16 km from the coast. The SARAL and model curves have more or less similar slopes but SARAL SSH begins to increase much further from the coast than the simulated SSH (70 km vs 50 km). On the contrary to Jason 2, the SARAL SSH variability is quite similar (std difference of 0.5 cm) to the simulated one near the coast. The corresponding mean velocity profiles have similar shapes, but slightly more spreaded offshore for altimetry (Fig. 5~~6~~d). The SARAL-derived currents are less noisy than Jason 2 ones but with still greater variability than the model reference (std of 0.16 m s^{-1} for SARAL raw data, and 0.068 m s^{-1} for the model). They are also closer to the currents derived from the MDT.

Finally, we repeated the process for Sentinel-3 (Fig. 5~~6~~e,f). As explained before, the model is shifted in time in order to have enough data to compute statistics. In terms of SSH profile (Fig. 5~~6~~e), Sentinel-3 appears very similar to SARAL (Fig. 5~~6~~c). SSH increases further south for the observations than for the model, leading to a slightly more offshore extended current. Compared to Jason 2 and SARAL, Sentinel-3 1-Hz data get much closer to the coast (around 1 km), and are also less noisy with SSH standard deviation quite identical to the model near the coast and slightly higher far from the coast. Figure 5~~6~~f shows that, thanks to its better coastal data coverage, Sentinel-3 captures the NC almost entirely. The current variability remains quite important along the track compared to the model (0.19 m s^{-1} for altimetry against 0.065 m s^{-1} for the model in average) and a huge standard deviation value characterizes the first point near the coast.

From the results of Fig. 5~~6~~, we computed the time-averaged NC characteristics (SSH drop, NC width and distance to the coast of the NC core). The results are summarized in Table 3~~2~~. For Jason 2, the NC signature in SSH is significantly stronger than that seen by the model sampled as altimetry: 10.2 cm and 7.2 cm respectively. This is mainly due to the divergence between the model and altimetry SSH near the coast. SARAL is very close to the model: 7.1 cm against 6.8 cm. Sentinel-3 is in between, with a drop of 8.2 cm vs 6.8 cm for the model. The NC width is slightly larger in altimetry than in the model (+6/+5/+1 km for Jason-2/SARAL/Sentinel-3, respectively). In Jason-2 and Sentinel-3, the NC core is located at the same distance to the coast as in the model, but it is located 8 km further from the coast in SARAL. Note that Sentinel-3 data better matches the model outcomes in two (i.e. NC width and core location) of the three analyzed diagnostics, while SARAL is closer to the model estimation of the SSH drop~~Note also that the NC is better (almost entirely) resolved in Sentinel-3, compared to Jason-2 and SARAL.~~

4.2 The altimetry data filtering issue

In practice, users systematically apply a spatial filter to altimetry SLA~~SSH~~ data before geostrophic current derivation~~, an operation that strongly amplifies~~ in order to remove the measurement noise~~, as~~ observed in section 4.1. The SLA ~~SSH~~ filtering step is then a key element of altimetry current computation and it is even more true in coastal areas. Consequently, the capability of altimetry to capture mesoscale currents depends on the choice of the filter.

Figure 6~~7~~ illustrates this noise issue by presenting the ~~time space~~Hovmöller diagrams ~~diagram~~ of SSH derived from the model and from 1-Hz altimetry raw data along the Jason 2 track 222 in the 120 km close to the coast. Note that with Jason-2, due to editing because of the noise~~for the reason explained before~~, near-shore data are often missing. If the evolution of both SSH fields is globally similar, we clearly observe noise in altimetry data as well as larger differences near the coast (i.e. in the first 30 km).

To estimate the best SLA ~~SSH~~ filtering for the derivation of current estimates, we compute the distribution of the resulting geostrophic velocity values, using raw and low-pass filtered SLA ~~SSH~~ altimetry data added to the MDT in the 60 km close to the coast. We compare the results to the distribution of the corresponding model velocities, used here again as a reference. To obtain the filtered SSH, we tested different cutoff frequencies on SLA data, ranging from 30 km to 50 km for SARAL and Sentinel-3 and extending to 70 km for Jason 2, and then added the MDT. Indeed, Morrow et al. (2017) and Raynal et al. (2017) showed a greater noise level in Jason 2 which required larger cutoff frequency values. The histograms of current values are represented in Fig. 8 for Jason 2 track 222, in Fig. 9 for SARAL track 302 and in Fig. 10 for Sentinel-3 track 472 (altimetry in blue superposed on the model in pink). Note that for each mission, the model current values are sampled at altimetry temporal resolution (10, 35 and 27 days for Jason 2, SARAL and Sentinel-3 respectively) and at the model resolution to investigate the impact of undersampling data (bottom figures). Table 3 summarizes the statistics derived from the histograms: the median, the standard deviation, as well as the number of points outside typical current values in this area and considered as outliers (greater than 0.25 m s^{-1} and smaller than -0.6 m s^{-1}. These values are considered the typical NC velocities). Here the distribution represents the variability of the current and the objective is to be as close as possible to the current variability shown by the model

We first focus on Jason 2. The model reference shows a distribution which tends to be gaussian. It is centered around -0.15 m s^{-1}, with a majority of negative values and is slightly asymmetric. Jason-2 raw velocity values are almost randomly distributed. When Jason-2 SLA

SSH data are filtered, and as the cutoff wavelength increases, the histogram's distributions change and get closer to the model ones. Regarding the statistics (Table 3), the too high standard deviation and too negative median values in the raw Jason-2 data get closer to the reference with the increase in cutoff wavelength. With a 60 km - filtering, we have the same standard deviation values in both Jason-2 and model velocities but the median value remains always significantly lower in Jason-2. The number of outliers is also too large in raw Jason-2 data, but decreases rapidly with the filtering; it is the closest to the model reference for a 60 km - filtering. From these results we conclude that Jason 2 currents tend to best converge towards the model reference with a filtering at 60 km. Beyond this cutoff wavelength, the smoothing erases the left and right-hand sides of the distribution (Fig. 8) and reduces the variability.

We repeat the same analysis with SARAL (Fig. 9 and Table 3). Note that there are fewer satellite cycles for SARAL than for Jason 2, so less current data are available to compute statistics. As a result, the distributions obtained are more complex than for Jason-2. It is clearly observed when comparing Fig. 9e and f (distributions computed at the model resolution and at a 35-day resolution). The model histogram is initially centered on -0.07 m s^{-1} with an asymmetric shape and a slight secondary peak around -0.25 m s^{-1}. When using the SARAL temporal resolution, the distribution is more random with a peak around -0.07 m s^{-1}. The raw altimetry solution is less randomly distributed than for Jason 2, also confirmed by a standard deviation value 2 times smaller than for Jason-2, 0.18 m s^{-1} vs 0.36 m s^{-1} and already relatively close to the 0.15 m s^{-1} model reference. SARAL tends to converge towards the model with a filtering of 30 km.

For Sentinel-3, the distribution of the raw altimetry solution has a bimodal shape (Fig. 10a) as in the model. Its standard deviation is also largely closer to the model reference, compared to Jason-2 (but slightly less than SARAL, Table 3). The statistics of the altimetry velocities tend to converge towards the model reference with a 40-50-km cutoff wavelength. One of the reasons for the slightly bimodal distribution in SARAL and Sentinel-3 may be the track orientation, quite different from the Jason 2 track which is perpendicular to the NC (Fig. 2e). Testing different track angles with the model reveals indeed a small second peak (not shown).

Note that the values obtained in this study are slightly lower than the numbers given in Raynal et al. (2017): ~70 km for Jason-2 and 35-50 km for SARAL/AltiKa and Sentinel 3, even if these studies focused on open ocean data. Morrow et al. (2017) also found values similar to Raynal et al. (2017) for Jason 2 and SARAL missions through spectral analysis.

Figure 10 shows the Hovmöller diagrams of the geostrophic currents obtained after filtering with the optimal values found previously for each mission. Fig. 10a along Jason 2 track 222 and 10b along SARAL track 302 include the model as the period is the same on the contrary to Sentinel-3 (Fig. 10c). We focus on the first 60 km to the coast as it corresponds to the NC. Fig. 10a confirms that the NC is not fully resolved by Jason 2 (bottom panel). The model geostrophic current shown on the top panel indicates seasonal variations of the amplitude, width and location of the NC. These seasonal variations are partly reproduced by the filtered altimetry solution, especially for 2012 and 2013. In 2014, strong values in summer are visible both in the model and in Jason 2.

The geostrophic currents derived from SARAL filtered data are shown on Fig. 10b on bottom panel with the equivalent for the model on the top panel. Even with a less important filtering SARAL data are less noisy. The seasonal pattern with stronger values in winter and weaker values in summer is very clear in the model and can be seen also in altimetry. However here again the NC is not fully resolved due to the lack of the most coastal points.

By getting closer to the coast (Fig 10c) Sentinel-3 data offers a more complete view of the NC although some noisy values are found near the coast. The seasonal cycle is visible in 2017. With a repetitive cycle of 35 and 27 days respectively, SARAL and Sentinel-3 are however less adapted to observe these variations.

5. Summary and conclusion

In this study, we have presented a novel method to quantify the SSH signature of a narrow slope current, the NC~~orthern Current~~ in the NWMED~~orth Western Mediterranean Sea~~, and to define its observability in altimetry data. It is based on a high resolution numerical model, intensively validated against in situ glider and HF radars data, and then considered as a reference for satellite altimetry data analysis. We consider the SSH and related surface geostrophic currents in parallel, using three nadir-looking radar altimeters that employ different technologies: Jason-2, SARAL and Sentinel-3. ~~We investigate how the advances in performance of these altimeters (Vergara et al., 2019) improve the observation of the NC.~~

We show that in the HF radars covered region the NC has a clear signature in SSH, characterized by a sea level drop from offshore to the coast, generally centered at ~15-20 km to the coast, with a mean value at 6.14°E of 6.9 ± 2.2 cm and spreading over 18 ± 4 km. In winter, the SSH drops are generally stronger than in summer and then theoretically easier to detect for altimeters. ~~but in parallel, the NC width also tends to diminish~~ in winter~~, inducing opposite effects in terms of observability capability.~~ The NC is also clearly associated with high frequency variability (sections 2.3 and 3). ~~Sammari et al. (1995) have noticed a variability of the~~ NC ~~alongslope component of the NC between 10 and 20 days that altimetry does not allow to resolve.~~ These results confirm that as a narrow, variable and close to the coast current, the NC monitoring is an issue for satellite altimetry. It is also important to note here that, whatever~~despite~~ the intrinsic performances of the instruments, the temporal resolution of the missions is an important limitation~~very important factor for~~ to the observation of coastal currents like the NC. ~~And o~~On this point the advantage is for Jason-2, compared to SARAL and Sentinel-3 missions.~~and that the larger the temporal resolution of the mission, the greater the difficulty. This is particularly true for SARAL and Sentinel-3, regardless of the instrument performance.~~

We then analyze the NC signature in altimetry data in comparison to the model reference. Jason 2 and SARAL 1-Hz data stop at 8 and 16 km~~ more than 10 km~~ from~~to~~ the coast, respectively, sometimes preventing observation of the whole NC. Probably thanks to the SAR mode, it is better resolved in Sentinel-3, with data at 1 km to the coast. In average, the SSH drops associated with the NC are always overestimated ~~too high~~ in altimetry, with mean values of 3.6 cm, 0.3 and 1.4 cm larger for Jason 2, SARAL and Sentinel-3, respectively. The mean NC core location is correctly located in Jason 2 and Sentinel-3 but it is slightly shifted in SARAL (an 8 km difference between the model and observations). In terms of current variability, all altimetry missions show much higher values than the model, because of the measurement noise. But this overestimation decreases significantly from Jason-2 (3.7 times larger) to the more recent Sentinel-3 and SARAL missions~~ – have much lower values than Jason-2 (which remain 3.7 times larger than the model reference)~~. The values closest to the model reference are obtained with SARAL (2.4 times larger, against 2.9 for Sentinel-3). ~~These too high values are of course largely explained by the measurement noise, significantly decreasing in the most recent altimetry missions. In section 4.1, we observe how this noise reduction has a strong impact on the quality of velocity derived from SSH, with the best performance obtained with SARAL data.~~ However, ~~the signal-over-~~noise ~~ratio~~ remains too large and all satellite SSH data must clearly be filtered before computing currents. By comparing the distributions of altimetry velocity fields derived with different filtering strategies with the model reference, we find that the optimal cutoff wavelength is 60 km, 30 km and 40-50 km for Jason-2, SARAL and Sentinel-3 SSH data, respectively. ~~Note that these values are slightly lower than the numbers given in Raynal et al. (2017):~~ ~70 **km for Jason-2 and 35-50 km for SARAL/AltiKa and Sentinel□3, even if these studies focused on open ocean data. Morrow et al. (2017) also found values similar to Raynal et al. (2017) for Jason 2 and SARAL missions through spectral analysis.**

~~In summary, in terms of coastal circulation studies, the main advantages of Jason missions are the long time series (~30 years if we combine T/P and Jason-1,2,3 data) and its 10-day temporal resolution whereas its measurement noise, its large intertrack distance and its loss of coastal data are an issue. SARAL enables to strongly reduce the data noise and to have a much better spatial coverage but its temporal resolution and its loss of coastal data are negative points. Finally Sentinel-3 performs the best when approaching the coast and its SAR technique also allows to reduce the noise. However, it has a too low temporal resolution.~~ In summary, t~~T~~o ideally address the coastal observability question, future altimetry missions should combine instrumental improvements (Ka band and SAR altimetry as in SARAL and Sentinel-3) and the temporal resolution of Jason or better. Another ~~But a single altimeter mission can clearly not observe the complex range of coastal ocean variability and we should certainly define an~~ approach would be to better optimize~~d for the coastal ocean in order to mix~~ the use of data from the 9 missions flying simultaneously in

2021.

The method presented here can be easily transposed to other altimetry missions and other dynamical processes than the NC. As an example, we could also focus on eddy observability, studying the size, amplitude and spatial configuration of their signature in SSH, in comparison to the model reference. ~~More generally, this study illustrates the benefits of~~ U~~u~~Using a carefully calibrated high-resolution model as a reference for coastal altimetry studies~~. It~~ allows to overcome~~ming~~ the sc~~p~~arsity of independent observations ~~needed~~ to validate near-shore altimetry ~~observational~~ data. Models can be used as a reference to compare the performance of different altimetry missions, but also of ~~to compare or calibrate~~ different coastal data processing strategies. ~~And finally,~~ T~~t~~hey also provide 3D information on the whole range of ocean parameters that can be related to the sea level variations captured by altimetry.

Acknowledgements

This study was done with the financial support of the Region Occitanie and the CNES through their PhD funding programs. Altimetry data used in this study were developed, validated and distributed by the CTOH/LEGOS, France. Glider data were collected and made freely available by the Coriolis project (http://www.coriolis.eu.org) and programs that contribute. Support was provided by the French Chantier Méditerranée MISTRALS program (HyMeX and MERMeX components) and by the EU projects FP7 GROOM (grant agreement 284321), FP7 PERSEUS (grant agreement 287600), FP7 JERICO (grant agreement 262584) and the COST Action ES0904 EGO (Everyone's Gliding Observatories). The long-term monitoring of the Northern Current is part of the Mediterranean Ocean Observation Service for the Environment (MOOSE) with HF radars activities also supported by the EU H2020 infrastructure project JERICO-NEXT (2015-2019) and actually by EU Interreg Marittimo program SICOMAR- PLUS. We thank the Parc National de Port-Cros (PNPC), "Association Syndicale des Propriétaires du Cap Bénat" (ASPCB) and the Group Military Conservation and the Marine Nationale for hosting our radar installations. The simulation was performed using the HPC CALMIP platform under grant P09115 and GENCI and CINES (Grand Equipement National de Calcul Intensif, project A0040110088). The SYMPHONIE model is distributed by the SIROCCO group (https://sirocco.obs-mip.fr).

Bibliographie

Alberola, C., Millot, C., and Font, J.: On the seasonal and mesoscale variabilities of the Northern Current during the PRIMO-0 experiment in the western Mediterranean-sea, Oceanol Acta, 18, 163–192, 1995.

Birol, F. and Delebecque, C.: Using high sampling rate (10/20Hz) altimeter data for the observation of coastal surface currents: A case study over the northwestern Mediterranean Sea, J~~ournal of~~ Marine Syst~~ems~~, 129, 318–333, https://doi.org/10.1016/j.jmarsys.2013.07.009, 2014.

Birol, F., Cancet, M., and Estournel, C.: Aspects of the seasonal variability of the Northern Current (NW Mediterranean Sea) observed by altimetry, J~~ournal of~~ Marine Syst~~ems~~, 81, 297–311, https://doi.org/10.1016/j.jmarsys.2010.01.005, 2010.

Birol, F., Fuller, N., Lyard, F., Cancet, M., Niño, F., Delebecque, C., Fleury, S., Toublanc, F., Melet, A., Saraceno, M., and Léger, F.: Coastal applications from nadir altimetry: Example of the X-TRACK regional products, Adv~~ances in~~ Space Res~~earch~~, 59, 936–953, https://doi.org/10.1016/j.asr.2016.11.005, 2017.

Birol, F., Léger, F., Passaro, M., Cazenave, A., Niño, F., Calafat, F. M., Shaw, A., Legeais, J.-F., Gouzenes, Y., Schwatke, C., and Benveniste, J.: The X-TRACK/ALES multi-mission processing system: New advances in altimetry towards the coast, Adv~~ances in~~ Space Res~~earch~~, 67, 2398–2415, https://doi.org/10.1016/j.asr.2021.01.049, 2021.

Borrione, I., Oddo, P., Russo, A., and Coelho, E.: Understanding altimetry signals in the Northeastern Ligurian sea using a multi-platform approach, Deep Sea Res~~earch~~ P~~ar~~t I: Oceanographic Research Papers, 145, 83–96, https://doi.org/10.1016/j.dsr.2019.02.003, 2019.

Bouffard, J., Vignudelli, S., Herrmann, M., Lyard, F., Marsaleix, P., Ménard, Y., and Cipollini, P.: Comparison of Ocean Dynamics with a Regional Circulation Model and Improved Altimetry in the North-Western Mediterranean, Terr. Atmos. Ocean. Sci., 19, 117, https://doi.org/10.3319/TAO.2008.19.1-2.117(SA), 2008.

Carret, A., Birol, F., Estournel, C., Zakardjian, B., and Testor, P.: Synergy between in situ and altimetry data to observe and study Northern Current variations (NW Mediterranean Sea), Ocean Sci., 15, 269–290, https://doi.org/10.5194/os-15-269-2019, 2019.

Casella, E., Molcard, A., and Provenzale, A.: Mesoscale vortices in the Ligurian Sea and their effect on coastal upwelling processes, J~~ournal of~~ Marine Syst~~ems~~, 88, 12–19, https://doi.org/10.1016/j.jmarsys.2011.02.019, 2011.

Crépon, M., Wald, L., Monget, J. M.: Low-Frequency Waves in the Ligurian sea During December 1977, J Geophys Res, 87, 595-600, 10.1029/JC087iC01p00595, 1982

Damien, P., Bosse, A., Testor, P., Marsaleix, P., and Estournel, C.: Modeling Postconvective Submesoscale Coherent Vortices in the Northwestern Mediterranean Sea, J Geophys Res-Oceans, 122, 9937–9961, https://doi.org/10.1002/2016JC012114, 2017.

Dufau, C., Orsztynowicz, M., Dibarboure, G., Morrow, R., and Traon, P.-Y. L.: Mesoscale resolution capability of altimetry: Present and future, J Geophys Res-Oceans, 121, 4910–4927, https://doi.org/10.1002/2015JC010904, 2016.

Estournel, C., Broche, P., Marsaleix, P., Devenon, J. L., Auclair, F., Vehil, R.: The Rhone River Plume in Unsteady Conditions: Numerical and Experimental Results, Estuar Coast Shelf S, 53, 25-38, https://doi.org/10.1006/ecss.2000.0685, 2001

Estournel, C., Broche, P., Marsaleix, P., Devenon, J.L., Auclair, F. and Vehil, R, 2001 : The Rhone river plume in unsteady conditions : numerical and experimental results. Estuarine, Coastal and Shelf Science, 53, 25-38.

Estournel, C., Madron, X. D. de, Marsaleix, P., Auclair, F., Julliand, C., and Vehil, R.: Observation and modeling of the winter coastal oceanic circulation in the Gulf of Lion under wind conditions influenced by the continental orography (FETCH experiment), J Geophys Res-Oceans, 108, https://doi.org/10.1029/2001JC000825, 2003.

Estournel, C., Testor, P., Damien, P., D'Ortenzio, F., Marsaleix, P., Conan, P., Kessouri, F., Madron, X. D. de, Coppola, L., Lellouche, J.-M., Belamari, S., Mortier, L., Ulses, C., Bouin, M.-N., and Prieur, L.: High resolution modeling of dense water formation in the north-western Mediterranean during winter 2012–2013: Processes and budget, J Geophys Res-Oceans, 121, 5367–5392, https://doi.org/10.1002/2016JC011935, 2016.

Estournel, C., Marsaleix, P., and Ulses, C.: A new assessment of the circulation of Atlantic and Intermediate Waters in the Eastern Mediterranean, Prog Oceanogr, 198, 102673, https://doi.org/10.1016/j.pocean.2021.102673, 2021.

Flexas, M. M., Durrieu de Madron, X., Garcia, M. A., Canals, M., Arnau, P.: Flow variability in the Gulf of Lions during the MATER HFF experiment (March-May 1997), J Marine Syst, 33-34, 197-214, 10.1016/S0924-7963(02)00059-3, 2002

Fu, L. L. and Le Traon, P.-Y.: Satellite altimetry and ocean dynamics, Comptes Rendus Geoscience, 338, 1063–1076, https://doi.org/10.1016/j.crte.2006.05.015, 2006.

Gentil, M ., Estournel, C., Durrieu de Madron, X., Many, G., Miles, T., Marsaleix, P., Berné, S., Bourrin, F. Sediment dynamics on the outer-shelf of the Gulf of Lions during an onshore storm: an approach based on acoustic glider and numerical modelling. Continental Shelf Research, 240, 104721,https://doi.org/10.1016/j.csr.2022.104721, 2022.

Gourdeau, L., Verron, J., Chaigneau, A., Cravatte, S., and Kessler, W.: Complementary Use of Glider Data, Altimetry, and Model for Exploring Mesoscale Eddies in the Tropical Pacific Solomon Sea: MESOSCALE EDDIES IN THE SOLOMON SEA, J. Geophys. Res. Oceans, 122, 9209–9229, https://doi.org/10.1002/2017JC013116, 2017.

Grilli, F. and Pinardi N.: The computation of Rossby radii of deformation for the Mediterranean Sea. MTP news 6.6, p. 4–5. 1998

Guihou, K., Marmain, J., Ourmières, Y., Molcard, A., Zakardjian, B., and Forget, P.: A case study of the mesoscale dynamics in the North-Western Mediterranean Sea: a combined data–model approach, Ocean Dynamics, 63, 793–808, https://doi.org/10.1007/s10236-013-0619-z, 2013.

Herrmann, M., Somot, S., Sevault, F., Estournel, C., and Déqué, M.: Modeling the deep convection in the northwestern Mediterranean Sea using an eddy-permitting and an eddy-resolving model: Case study of winter 1986–1987, J Geophys Res 113, https://doi.org/10.1029/2006JC003991, 2008.

Hu, Z. Y., Petrenko, A. A., Doglioli, A. M., and Dekeyser, I.: Study of a mesoscale anticyclonic eddy in the western part of the Gulf of Lion, J~~ournal of~~ Marine Syst~~ems~~, 88, 3–11, https://doi.org/10.1016/j.jmarsys.2011.02.008, 2011.

Jebri, F., Birol, F., Zakardjian, B., Bouffard, J., and Sammari, C.: Exploiting coastal altimetry to improve the surface circulation scheme over the central Mediterranean Sea, J Geophys Res Oceans, 121, 4888–4909, https://doi.org/10.1002/2016JC011961, 2016.

Juza, M., Renault, L., Ruiz, S., and Tintoré, J.: Origin and pathways of Winter Intermediate Water in the Northwestern Mediterranean Sea using observations and numerical simulation, J Geophys Res Oceans, 118, 6621–6633, https://doi.org/10.1002/2013JC009231, 2013.

Lellouche, J.-M., Le Galloudec, O., Drévillon, M., Régnier, C., Greiner, E., Garric, G., Ferry, N., Desportes, C., Testut, C.-E., Bricaud, C., Bourdallé-Badie, R., Tranchant, B., Benkiran, M., Drillet, Y., Daudin, A., and De Nicola, C.: Evaluation of global monitoring and forecasting systems at Mercator Océan, Ocean Sci, 9, 57–81, https://doi.org/10.5194/os-9-57-2013, 2013.

Liu, J., Dai, J., Xu, D., Wang, J., and Yuan, Y.: Seasonal and Interannual Variability in Coastal Circulations in the Northern South China Sea, MDPI, 10, 520, https://doi.org/10.3390/w10040520, 2018.

Marsaleix P., Auclair F., Estournel C.: Considerations on Open Boundary Conditions for Regional and Coastal Ocean Models. J~~ournal of~~ Atmos~~pheric and~~ Ocean~~ic~~ Tech~~nology~~, 23,1604-1613, http://dx.doi.org/10.1175/JTECH1930.1, 2006

Marsaleix, P., Auclair, F., Floor, J. W., Herrmann, M. J., Estournel, C., Pairaud, I., and Ulses, C.: Energy conservation issues in sigma-coordinate free-surface ocean models, Ocean Model~~ling~~, 20, 61–89, https://doi.org/10.1016/j.ocemod.2007.07.005, 2008.

Michaud, H., Marsaleix, P., Leredde, Y., Estournel, C., Bourrin, F., Lyard, F., Mayet, C., and Ardhuin, F.: Three-dimensional modelling of wave-induced current from the surf zone to the inner shelf, Ocean Sci, 8, 657–681, https://doi.org/10.5194/os-8-657-2012, 2012.

Mikolajczak, G., Estournel, C., Ulses, C., Marsaleix, P., Bourrin, F., Martín, J., Pairaud, I., Puig, P., Leredde, Y., Many, G., Seyfried, L., and Durrieu de Madron, X.: Impact of storms on residence times and export of coastal waters during a mild autumn/winter period in the Gulf of Lion, Cont~~inental~~ Shelf Res~~earch~~, 207, 104192, https://doi.org/10.1016/j.csr.2020.104192, 2020.

Millot, C.: Circulation in the Western Mediterranean Sea, Oceanol~~ogica~~ Acta, 10, 143–148, 1987.

Morrow, R., Carret, A., Birol, F., Nino, F., Valladeau, G., Boy, F., Bachelier, C., and Zakardjian, B.: Observability of fine-scale ocean dynamics in the northwestern Mediterranean Sea, Ocean Sci, 13, 13–29, https://doi.org/10.5194/os-13-13-2017, 2017.

Niewiadomska, K., Couplage physique-biogéochimie à différentes échelles spatiales et temporelles : le cas du courant Ligure étudié par un planeur bio-optique sous-marin, Ph.D. thesis, Université Pierre et Marie Curie, France, 2008

Niewiadomska, K., Claustre, H., Prieur, L., and d'Ortenzio, F.: Submesoscale physical-biogeochemical coupling across the Ligurian current (northwestern Mediterranean) using a bio-optical glider, Limnol Oceanogr, 53, 2210, 2008.

Ourmières, Y., Zakardjian, B., Béranger, K., Langlais, C.: Assessment of a NEMO-based downscaling experiment for the North-Western Mediterranean region: Impacts on the Northern Current and comparison with ADCP data and altimetry products, Ocean Model, 39, 386-404, 2011

Pascual, A., Lana, A., Troupin, C., Ruiz, S., Faugère, Y., Escudier, R., and Tintoré, J.: Assessing SARAL/AltiKa Data in the Coastal Zone: Comparisons with HF Radar Observations, Mar Geod, 38, 260–276, https://doi.org/10.1080/01490419.2015.1019656, 2015.

Petrenko, A., Dufau, C., and Estournel, C.: Barotropic eastward currents in the western Gulf of Lion, north-western Mediterranean Sea, during stratified conditions, J~~ournal of~~ Marine Syst~~ems~~, 74, 406–428, https://doi.org/10.1016/j.jmarsys.2008.03.004, 2008.

Raynal, M., Labroue, S., Urien, S., Amarouche, L., Moreau, T., Boy, F., Féménias, P., and Bouffard, J.: Performances and assessment of Cryosat-2 and Sentinel-3A SARM over ocean inferred from existing ground processing chains. Paper presented at Ocean Surface Topography Science Team Meeting (OSTST) 2017, Miami FL, United States of America.

Rio, M.-H., Pascual, A., Poulain, P.-M., Menna, M., Barceló, B., and Tintoré, J.: Computation of a new mean dynamic topography for the Mediterranean Sea from model outputs, altimeter measurements and oceanographic in situ data, Ocean Sci, 10, 731–744, https://doi.org/10.5194/os-10-731-2014, 2014.

Sammari, C., Millot, C., and Prieur, L.: Aspects of the seasonal and mesoscale variabilities of the Northern Current in the western Mediterranean Sea inferred from the PROLIG-2 and PROS-6 experiments, Deep~~-~~ Sea Res~~earch~~ Par~~t~~ I~~: Oceanographic Research Papers~~, 42, 893–917, https://doi.org/10.1016/0967-0637(95)00031-Z, 1995.

Schaeffer, A., Molcard, A., Forget, P., Fraunié, P., and Garreau, P.: Generation mechanisms for mesoscale eddies in the Gulf of Lions: radar observation and modeling, Ocean Dynam~~ics~~, 61, 1587–1609, https://doi.org/10.1007/s10236-011-0482-8, 2011.

Schroeder, K., Haza, A. C., Griffa, A., Özgökmen, T. M., Poulain, P. M., Gerin, R., Peggion, G., and Rixen, M.: Relative dispersion in the Liguro-Provençal basin: From sub-mesoscale to mesoscale, Deep~~-~~ Sea Res~~earch~~ Par~~t~~ I~~: Oceanographic Research Papers~~, 58, 209–228, https://doi.org/10.1016/j.dsr.2010.11.004, 2011.

Taupier-Letage, I., and Millot, C.: General hydrodynamical features in the Ligurian Sea inferred from the DYOME experiment, Oceanol Acta, 9, 2, 1986

Tintoré, J., Pinardi, N., Álvarez-Fanjul, E., Aguiar, E, Álvarez-Berastegui, D., Bajo, M., Balbin, R., Bozzano, R., Buongiorno Nardelli, B., Cardin, V., Casas, B., Charcos-Llorens, M., Chiggiato, J., Clementi, E., Coppini, G., Coppola, L., Cossarini, G., Deidun, A., Deudero, S., D'Ortenzio, F., Drago, A., Drudi, M., El Serafy, G., Escudier, R., Farcy, P., Federico, I., Fernández, J. G., Ferrarin, C., Fossi, C., Frangoulis, C., Galgani, F., Gana, S., García Lafuente, J., García Sotillo, M., Garreau, P., Gertman, I., Gómez-Pujol, L., Grandi, A., Hayes, D., Hernández-Lasheras, J., Herut, B., Heslop, E., Hilmi, K., Juza, M., Kallos, G., Korres, G., Lecci, R., Lazzari, P., Lorente, P., Liubartseva, S., Louanchi, F., Malacic, V., Mannarini, G., March, D., Marullo, S., Mauri, E., Meszaros, L., Mourre, B., Mortier, L., Muñoz-Mas, C., Novellino, A., Obaton, D, Orfila, A., Pascual, A., Pensieri, S., Pérez Gómez, B., Pérez Rubio, S., Perivoliotis, L., Petihakis, G., Petit de la Villéon, L., Pistoia, J., Poulain, P. M., Pouliquen, S., Prieto, L., Raimbault, P., Reglero, P., Reyes, E., Rotllan, P., Ruiz, S., Ruiz, J., Ruiz, I., Ruiz-Orejón, L. F., Salihoglu, B., Salon, S., Sammartino, S., Sánchez Arcilla, A., Sánchez-Román, A., Sannino, G., Santoleri, R., Sardá, R., Schroeder, K., Simoncelli, S., Sofianos, S., Sylaios, G., Tanhua, T., Teruzzi, A., Testor, P., Tezcan, D., Torner, M., Trotta, F., Umgiesser, G., von Schuckmann, K., Verri, G., Vilibic, I., Yucel, M., Zavatarelli, M., and Zodiatis, G.: Challenges for Sustained Observing and Forecasting Systems in the Mediterranean Sea, Frontiers in Marine Science, DOI: 10.3389/fmars.2019.00568, 2019

Troupin, C., Pascual, A., Valladeau, G., Pujol, I., Lana, A., Heslop, E., Ruiz, S., Torner, M., Picot, N., and Tintoré, J.: Illustration of the emerging capabilities of SARAL/AltiKa in the coastal zone using a multi-platform approach, Advances in Space Research, 55, 51–59, https://doi.org/10.1016/j.asr.2014.09.011, 2015.

Vergara, O., Morrow, R., Pujol, I., Dibarboure, G., and Ubelmann, C.: Revised Global Wave Number Spectra From Recent Altimeter Observations, J Geophys Res Oceans, 124, 3523–3537, https://doi.org/10.1029/2018JC014844, 2019.

Verron, J., Bonnefond, P., Aouf, L., Birol, F., Bhowmick, S. A., Calmant, S., Conchy, T., Crétaux, J.-F., Dibarboure, G., Dubey, A. K., Faugère, Y., Guerreiro, K., Gupta, P. K., Hamon, M., Jebri, F., Kumar, R., Morrow, R., Pascual, A., Pujol, M.-I., Rémy, E., Rémy, F., Smith, W. H. F., Tournadre, J., and Vergara, O.: The Benefits of the Ka-Band as Evidenced from the SARAL/AltiKa Altimetric Mission: Scientific Applications, Remote Sens 10, 163, https://doi.org/10.3390/rs10020163, 2018.

Vignudelli, S., Cipollini, P., Astraldi, M., Gasparini, G. P., and Manzella, G.: Integrated use of altimeter and in situ data for understanding the water exchanges between the Tyrrhenian and Ligurian Seas, J Geophys Res Oceans, 105, 19649–19663, https://doi.org/10.1029/2000JC900083, 2000.

Vignudelli, S., Kostianoy, A.G., Cipollini, P., Benveniste, J.: Coastal Altimetry, Springer, Berlin Heidelberg, 578 pp, doi:10.1007/978-3-642-12796-0. 2011

Zakardjian, B. and Quentin, C.: MOOSE HF radar daily averaged surface currents from MEDTLN site (Toulon NW Med), SEA-NOE, https://doi.org/10.17882/56500, 2018.

	Altimetry mission		
	Jason 2	SARAL	Sentinel-3

Track used	222	302	472
Data period	June 2008 - October 2016	April 2013 - May 2016	June 2016 - May 2019
Intertrack distance in the NW MedSea	230 km	58 km	78 km
Temporal resolution	10 days	35 days	27 days
Radar technology	Conventional LRM altimetry - Ku band	Conventional LRM altimetry - Ka band	SAR altimetry - Ku band
Along-track resolution at 1-Hz	5.8 km	7.5 km	6.7 km
Number of sampled used	195	32	36
SSH RMS (Vergara et al., 2019)	2.23 cm	1.66 cm	1.12 cm

Table 1: Characteristics of the altimetry datasets used in this study as a function of the satellite mission.

	NC Core (°)	*NC width (km)*	*NC maximum amplitude (m.s-1)*
HF radars	*42.85*	*18 +/- 6.1*	*-0.43 +/- 0.19*
Model	*42.85*	*18 +/- 5.9*	*-0.44 +/- 0.16*
Gliders	*43.52*	*30 +/- 9.6*	*-0.25 +/- 0.13*
Model	*43.51*	*24 +/- 6.6*	*-0.23 +/- 0.12*

Table 2: Characteristics of the Northern Current along HF radars and gliders sections

Dataset	SSH drop (cm)	NC width (km)	Distance to the coast of the NC core (km)	Period considered for the statistics
Jason 2 track 222	10.2	33	27	27/05/2011 - 01/10/2016
SYMPHONIE	6.6	27	27	
SARAL track 302	7.1	25	20	24/03/2013 -

SYMPHONIE	6.8	20	12	13/03/2016
Sentinel-3 track 472	8.2	29	17	18/06/2016 - 14/03/2019
SYMPHONIE	6.8	28	17	21/06/2014 - 15/03/2017

Table 3~~2~~: Northern Current SSH signature derived from~~based on~~ the time averaged SSH profiles computed along the Jason 2 track 222, the SARAL track 302, the Sentinel-3 track 472 and the equivalent SYMPHONIE sampled as 1-Hz altimetry: SSH drop, NC width and distance to the coast ~~computed for the Jason 2 track 222, the SARAL track 302, the Sentinel-3 track 472 and SYMPHONIE sampled as 1-Hz altimetry~~.

	Mission	standard deviation m s-1	median m s-1	number of points >0.25m s^{-1} or <-0.6 m s^{-1}
model (daily)	Jason 2	0.14 (0.14) ~~m s^{-1}~~-	-0.17 (-0.16) ~~m s^{-1}~~	6 (16)
	SARAL	0.15 (0.14) ~~m s^{-1}~~	-0.16 (-0.16) ~~m s^{-1}~~	0 (16)
	Sentinel-3	0.13 (0.13) ~~m s^{-1}~~	-0.17 (-0.16) ~~m s^{-1}~~	0 (1)
raw	Jason 2	0.36 ~~m s^{-1}~~	-0.20 ~~m s^{-1}~~	342
	SARAL	0.18 ~~m s^{-1}~~	-0.22 ~~m s^{-1}~~	7
	Sentinel-3	0.23 ~~m s^{-1}~~	-0.19 ~~m s^{-1}~~	18
filtering at 30 km	Jason 2	0.23 ~~m s^{-1}~~	-0.21 ~~m s^{-1}~~	104
	SARAL	0.14 ~~m s^{-1}~~	-0.19 ~~m s^{-1}~~	1
	Sentinel-3	0.17 ~~m s^{-1}~~	-0.20 ~~m s^{-1}~~	8
filtering at 40 km	Jason 2	0.19 ~~m s^{-1}~~	-0.21 ~~m s^{-1}~~	52
	SARAL	0.13 ~~m s^{-1}~~	-0.19 ~~m s^{-1}~~	1
	Sentinel-3	0.14 ~~m s^{-1}~~	-0.20 ~~m s^{-1}~~	4
filtering at 50 km	Jason 2	0.16 ~~m s^{-1}~~	-0.21 ~~m s^{-1}~~	15
	SARAL	0.11 ~~m s^{-1}~~	-0.19 ~~m s^{-1}~~	0
	Sentinel-3	0.13 ~~m s^{-1}~~	-0.20 ~~m s^{-1}~~	3
filtering at 60 km	Jason 2	0.14 ~~m s^{-1}~~	-0.20 ~~m s^{-1}~~	9
filtering at 70 km	Jason 2	0.12 ~~m s^{-1}~~	-0.20 ~~m s^{-1}~~	1

Table 3: Statistics corresponding to the distributions shown on Fig. 8, 9 and 10.

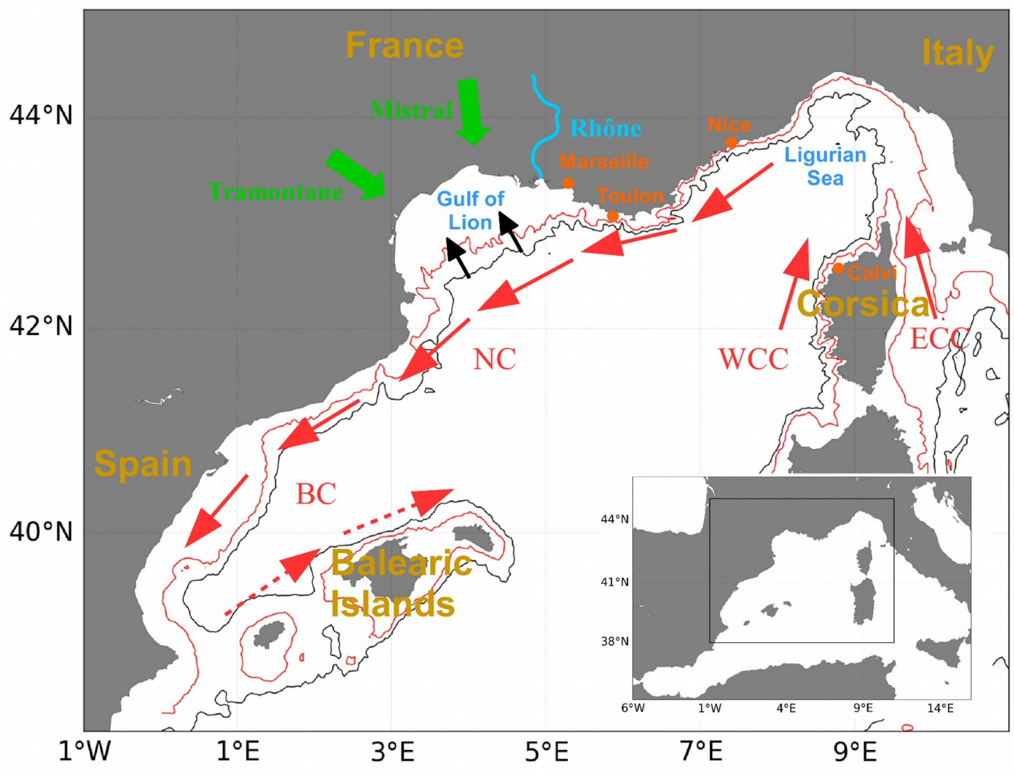

Figure 1: Map of the schematic circulation in the North-Western Mediterranean study area, with inset map showing the location of the main map (outlined by a black box). Red arrows indicate the main currents; black arrows indicate the intrusion in the Gulf of Lion. 200 m (red line) and 1000 m (black line) isobaths are also shown. The geographic features mentioned in the text are indicated. NC = Northern Current ; BC = Balearic Current ; WCC = Western Corsica Current ; ECC = Eastern Corsica Current

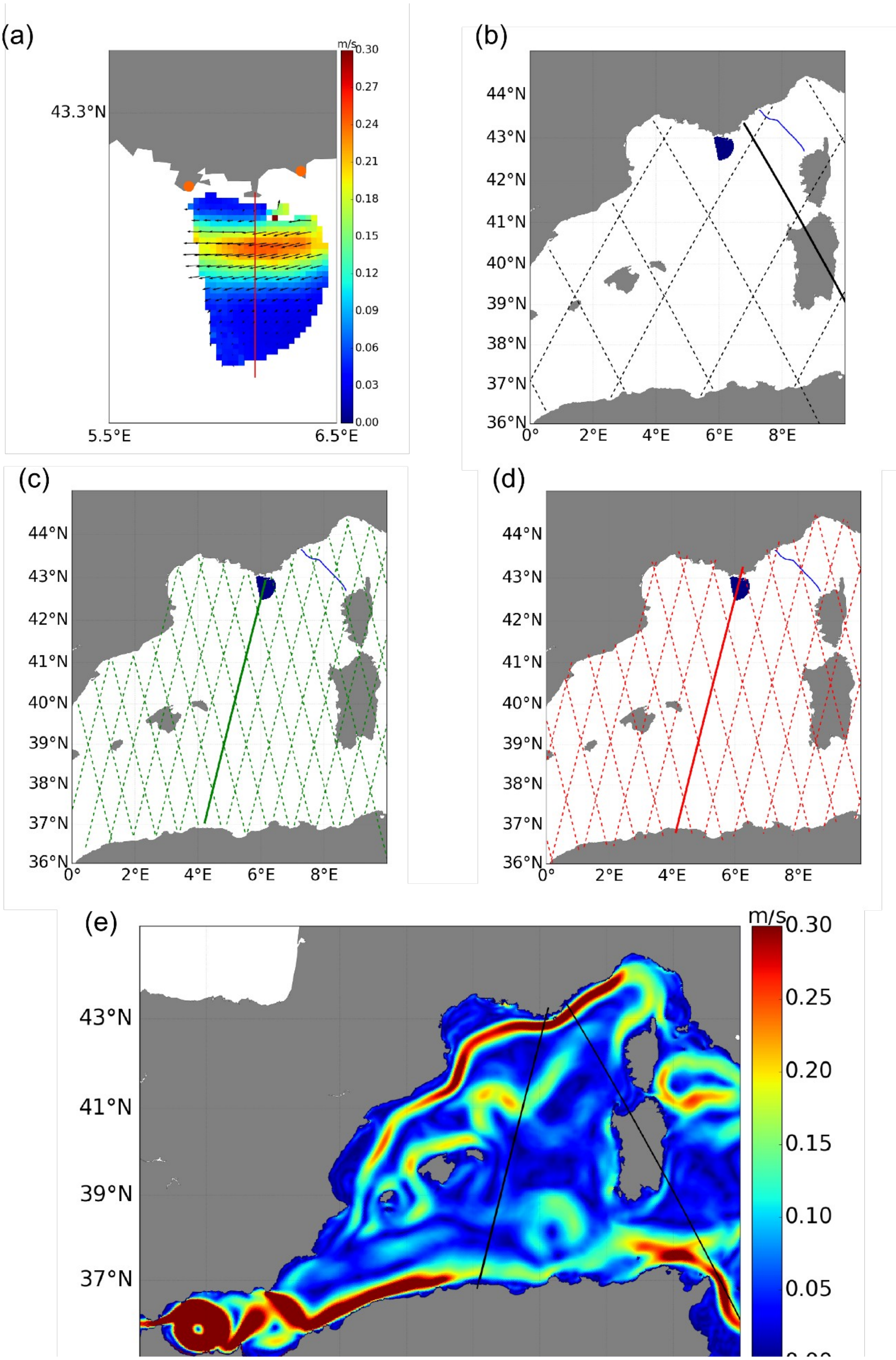

(a)
m/s
0.30
0.27
0.24
0.21
0.18
0.15
0.12
0.09
0.06
0.03
0.00
43.3°N
5.5°E
6.5°E
(b)
44°N
43°N
42°N
41°N
40°N
39°N
38°N
37°N
36°N
0°
2°E
4°E
6°E
8°E
(c)
(d)
(e)
m/s
0.30
0.25
0.20
0.15
0.10
0.05
43°N
41°N
39°N
37°N

Figure 2: Maps illustrating the location of the observations used in this study as well as the spatial model coverage. (a) Mean surface current velocity map from the HF radars near Toulon over 01/05/2012 to 30/09/2014; the red line shows the transect used in the study and the orange dots the location of the antennas. Altimetry tracks in the Western Mediterranean Sea for (b) Jason 2; (c) SARAL; (d) Sentinel-3. For each mission, the tracks used in the study (track 222 for Jason 2; track 302 for SARAL; track 472 for Sentinel-3) are indicated in bold. The HF radars coverage area and the Nice-Calvi glider transect are represented in blue. (e) Mean surface current intensity from the SYMPHONIE model for the period 18/05/2011-31/03/2017. The satellite tracks are represented in black.

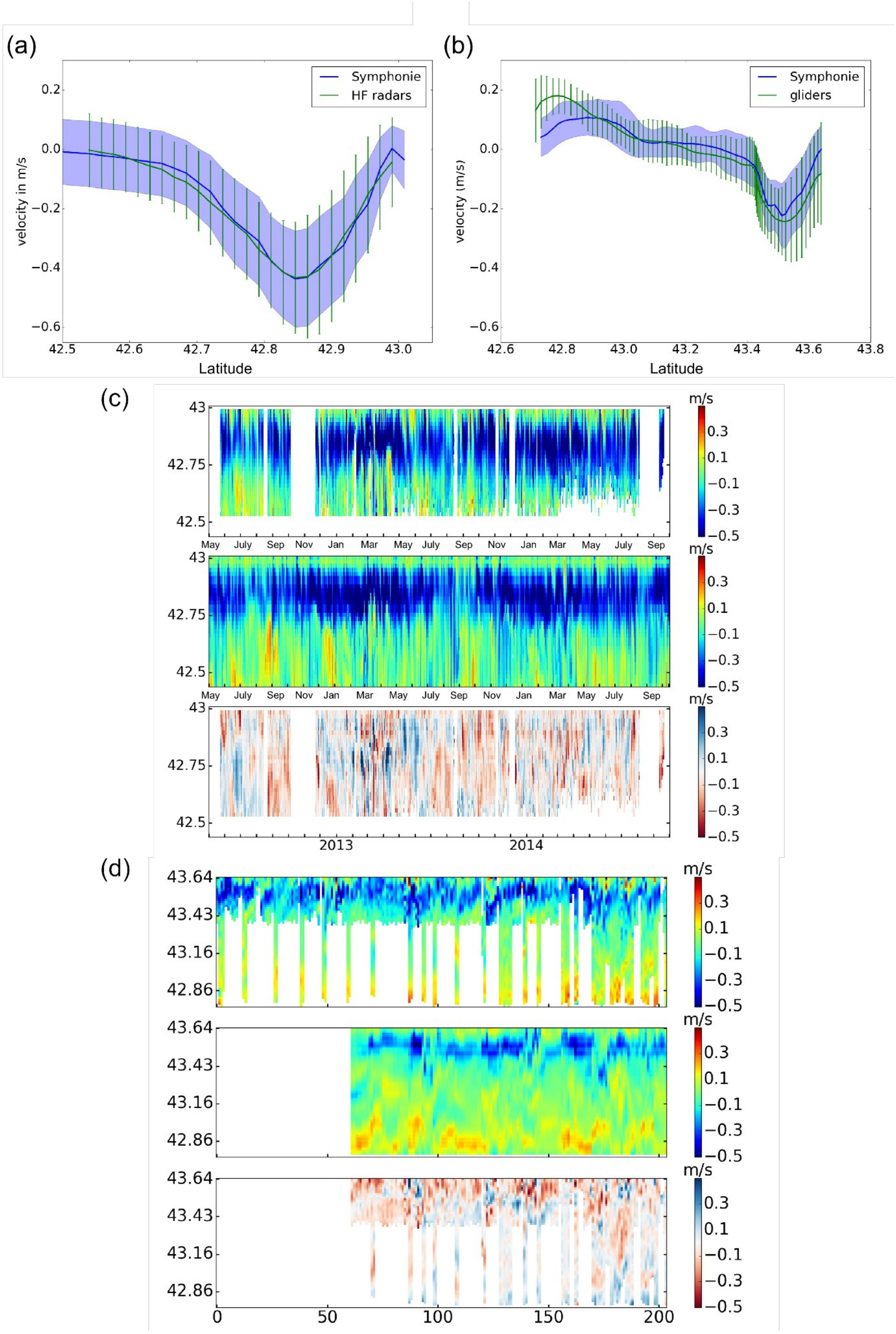

(a)
Symphonie
HF radars
velocity in m/s
Latitude
(b)
Symphonie
gliders
velocity (m/s)
Latitude
(c)
m/s
2013
2014
(d)
m/s

Figure 3: (a) Mean zonal total surface current velocities along a meridional section located at 6.14° E for the simulation in blue and the HF radars in green over the HF radars period: 01/05/2012 - 30/09/2014 ; (b) Mean across-track geostrophic current along the Nice-Calvi line for the simulation in blue and the gliders in green over 01/01/2011 - 31/12/2017. The blue envelope and the green bars represent the standard deviation at each point for the model and instruments respectively. Hovmöller diagrams of (c) the zonal total current component along a meridional section located at 6.14° E given by the HF radars (top panel) and the simulation (middle panel) ; (d) the geostrophic current for the gliders (top panel) and the simulation at the glider temporal resolution (middle panel). Lower panels of (c) and (d) show the differences between the observations and the simulation.

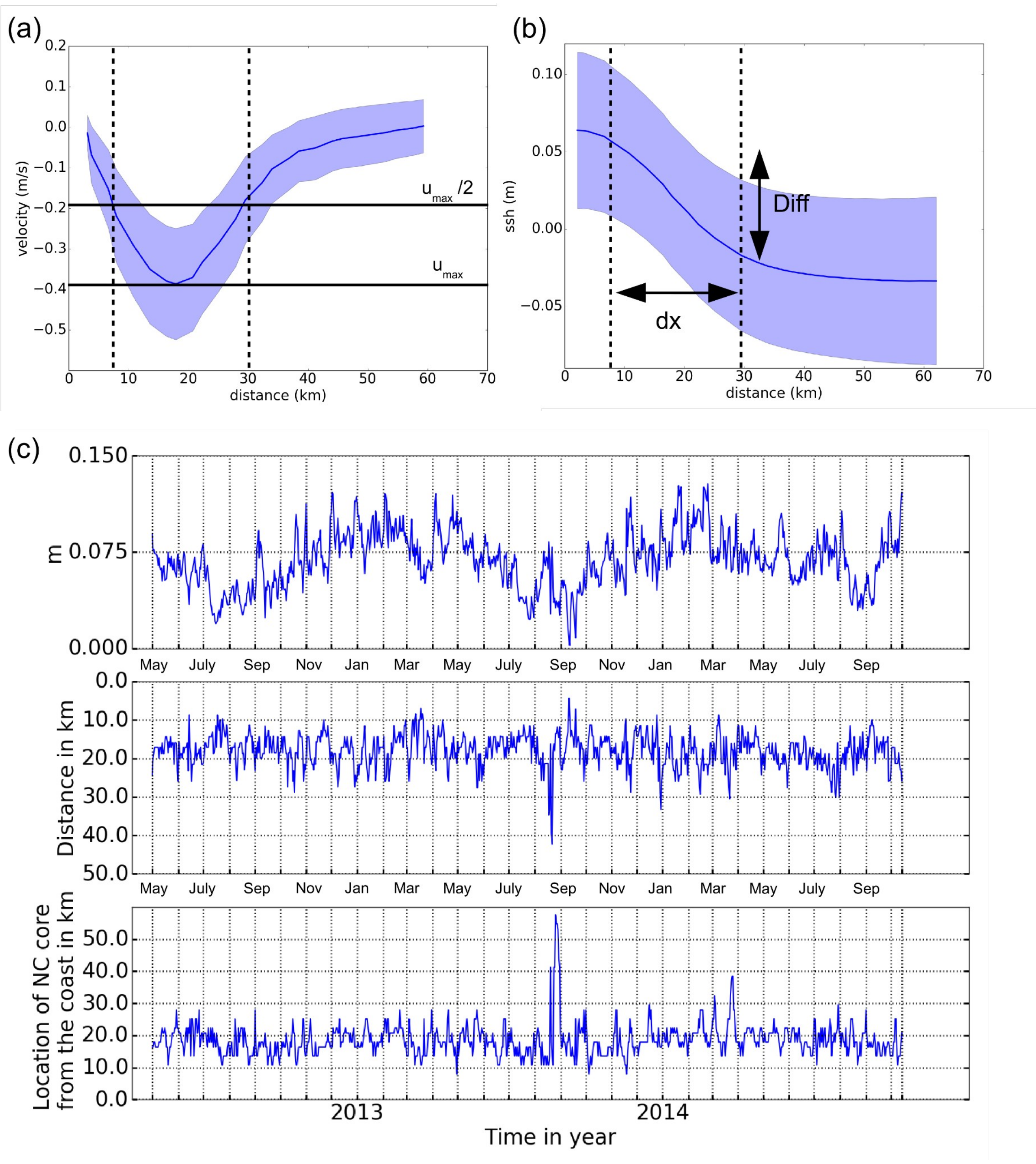

Figure 4~~5~~: Time averaged (a) surface current velocities and (b) SSH along a meridional *section located at 6.14° E for the SYMPHONIE model over the HF radars period: 01/05/2012 - 30/09/2014.(c) Time series of the SSH drop (in m, upper panel), width (in km, middle panel) of the NC , and location of the NC core as a function of the distance to the coast (in km, lower panel). The blue envelope in (a) and (b) represent the standard deviation at each point. The horizontal full lines correspond to the maximum and half the maximum velocity values. The dashed vertical lines delimit the NC width.*

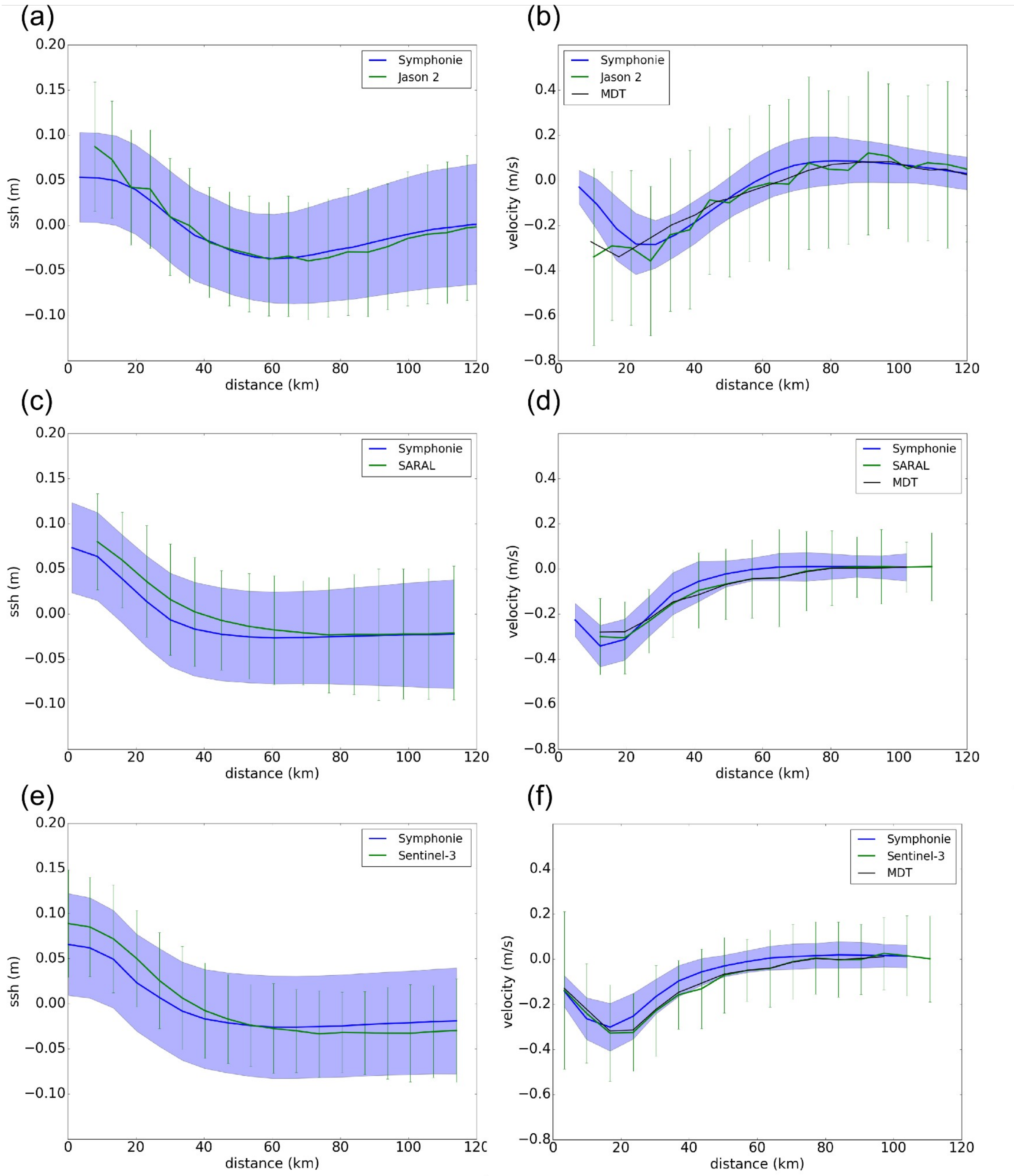

Figure 5: Mean (a), (c), (e) SSH and (b), (d), (f) across-track geostrophic current velocities along (a),

(b) Jason 2 track222 over 27/05/2011 - 01/10/2016; (c), (d) SARAL track 302 over 24/03/2013 - 13/03/2016; (e), (f) Sentinel-3 track 472 for the model over 21/06/2014 - 15/03/2017 in blue and altimetry raw data over 18/06/2016 - 14/03/2019 in green. The blue envelope and green bars represent the standard deviation at each point for the model and the satellite data, respectively. The distance is referenced to the coast.

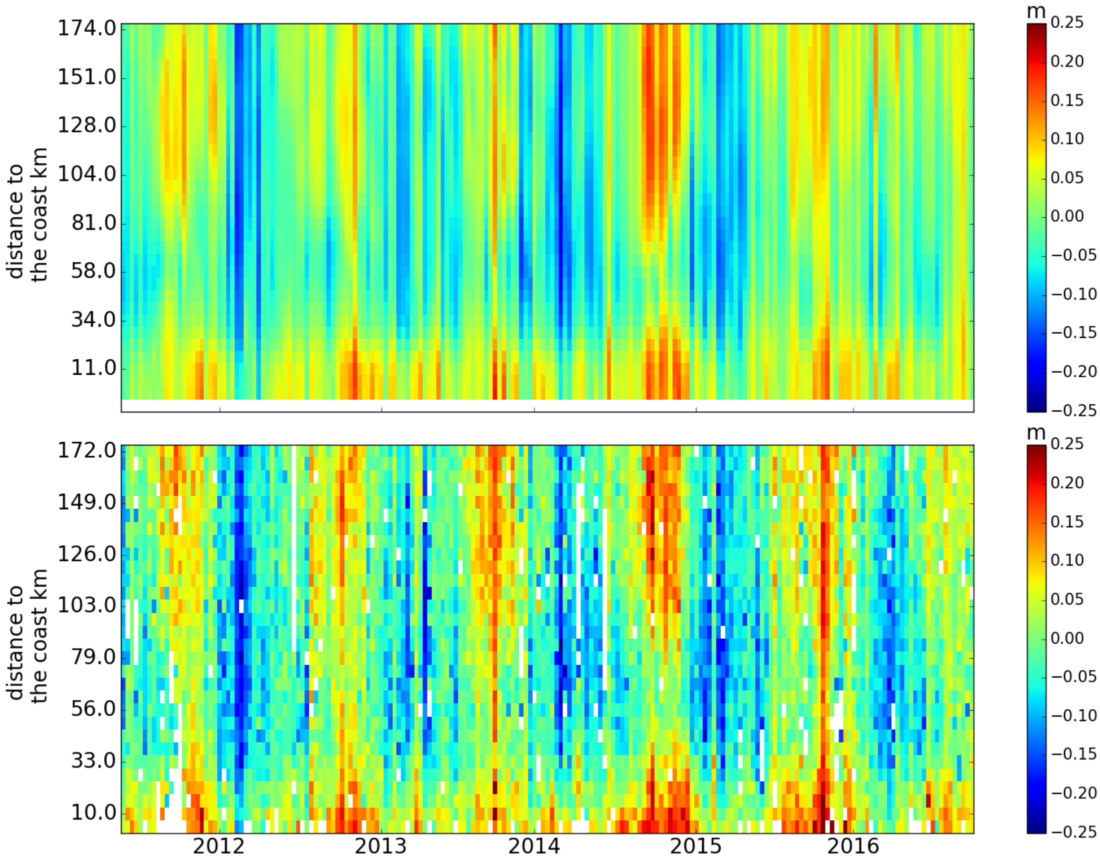

Figure 6: Hovmöller diagrams of SSH along the Jason 2 track 222 for the model (upper panel) and for Jason 2 (lower panel), as a function of the distance to the coast over the period 27/05/2011 - 01/10/2016.

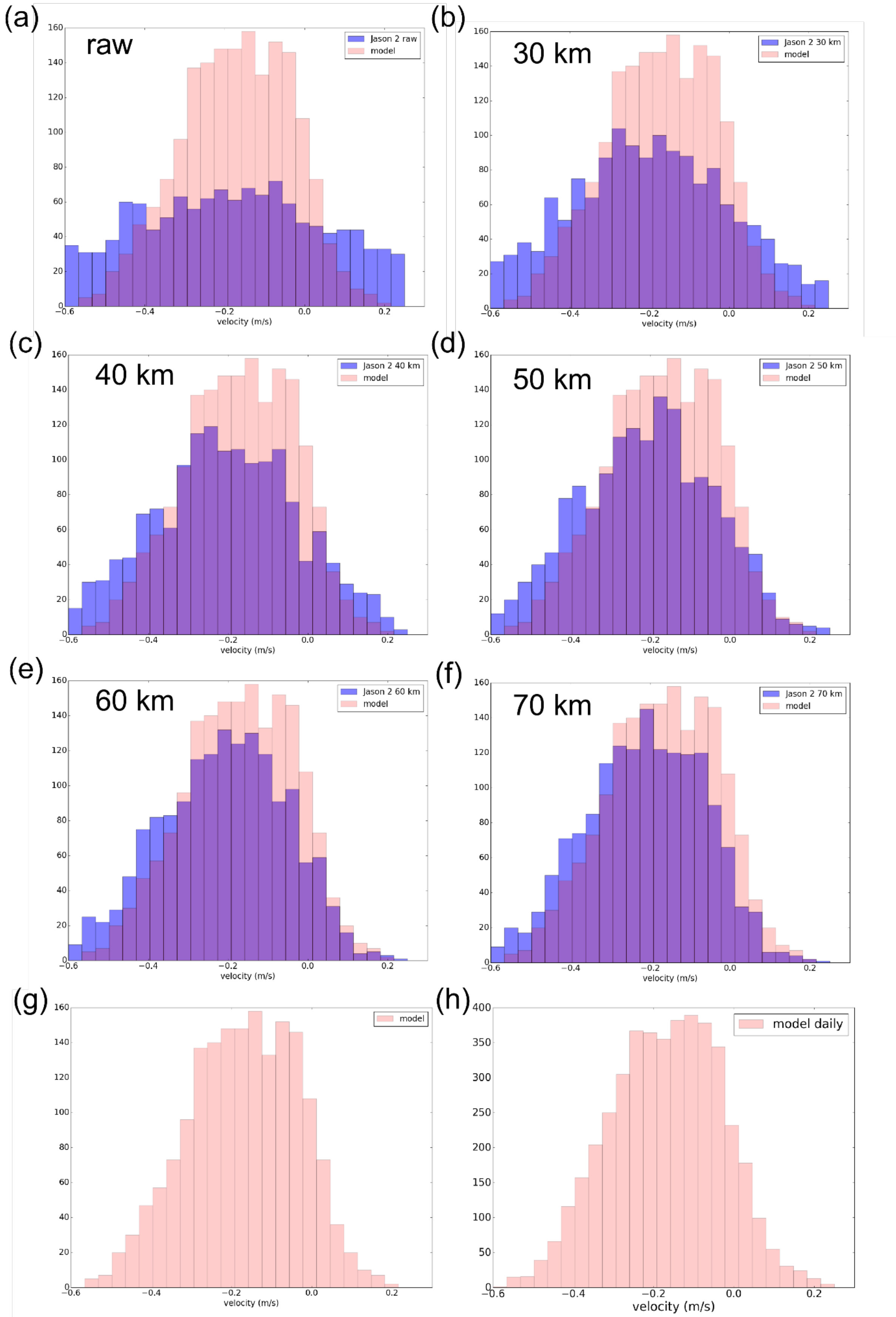
(a)
raw
Jason 2 raw
model
velocity (m/s)
(b)
30 km
Jason 2 30 km
model
velocity (m/s)
(c)
40 km
Jason 2 40 km
model
velocity (m/s)
(d)
50 km
Jason 2 50 km
model
velocity (m/s)
(e)
60 km
Jason 2 60 km
model
velocity (m/s)
(f)
70 km
Jason 2 70 km
model
velocity (m/s)
(g)
model
velocity (m/s)
(h)
model daily
velocity (m/s)

Figure 78: Distribution of the geostrophic current values along the Jason 2 track 222 and over the first 60 km to the coast over 27/05/2011 - 01/10/2016 for (a) raw altimetry data and (b),(c),(d),(e),(f) low-pass filtered altimetry data with different cutoff frequencies indicated in the panels. Altimetry distributions (in blue) are superimposed on the corresponding model distribution (in pink). The latter is computed for theJason 2 temporal resolution (g) and for the model resolution (h)

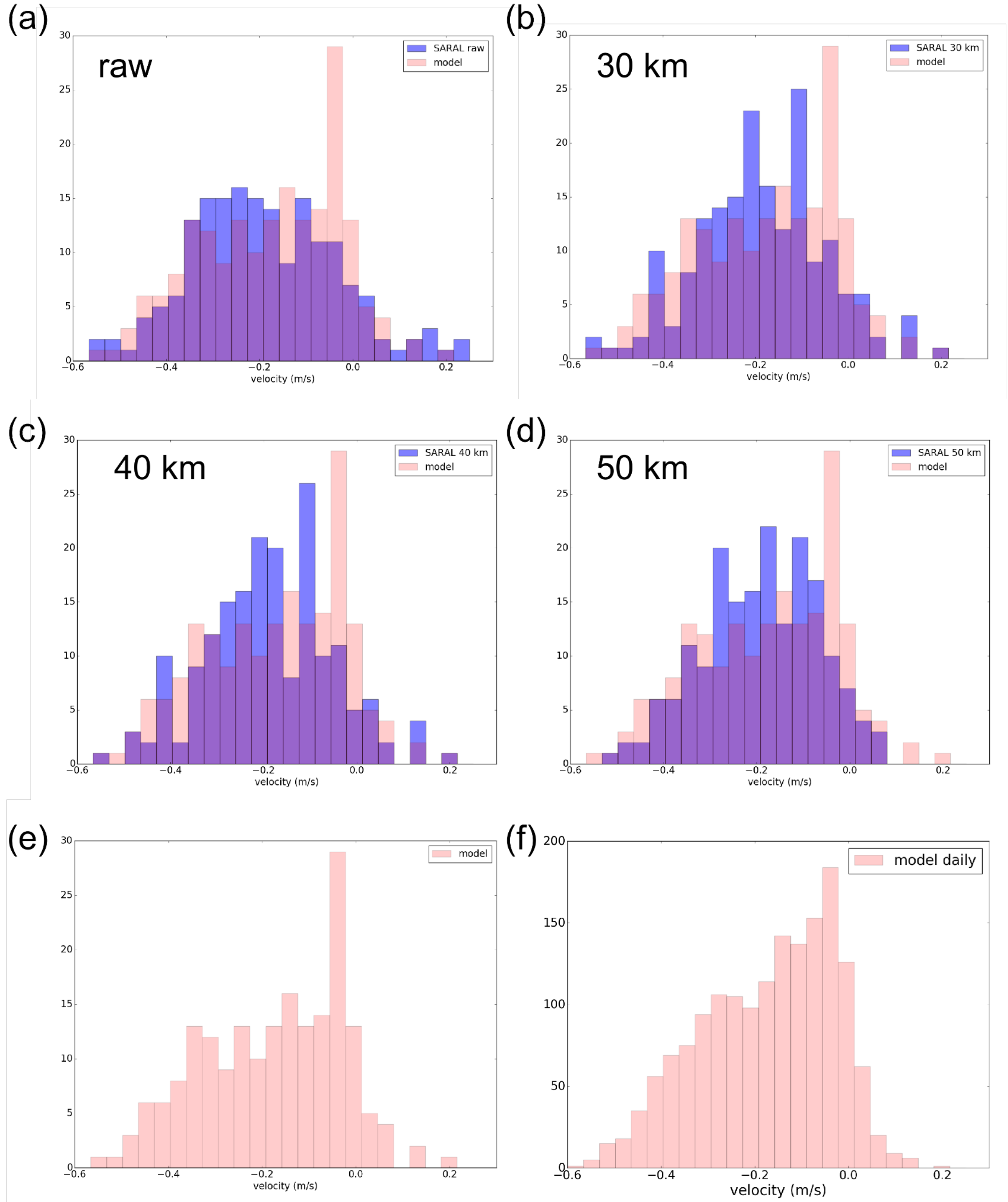

Figure 89: Distribution of the geostrophic current values along the SARAL track 302 and over the first 60 km to the coast over 24/03/2013 - 13/03/2016 for (a) raw altimetry data and (b),(c),(d),(e),(f) different filters indicated on each panel. Altimetry distribution (in blue) is superimposed on the

corresponding model distribution (in pink). The latter is computed for the SARAL temporal resolution (g) and for the model resolution (h)

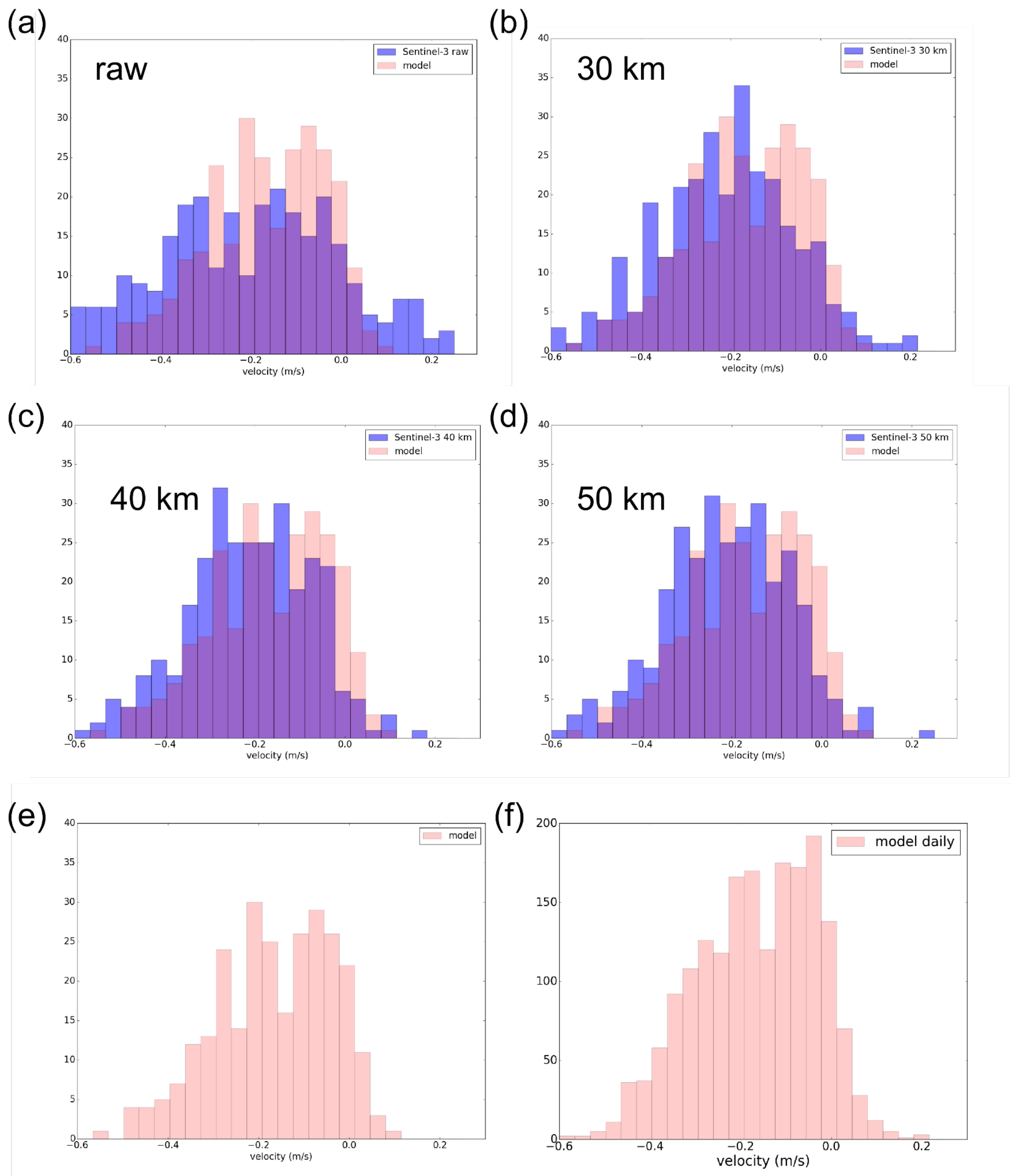

Figure 9 ~~10~~: Distribution of the geostrophic current values along the Sentinel-3 track 472 and over the first 60 km to the coast for (a) raw altimetry data and (b),(c),(d),(e),(f) different filters (in blue).Altimetry distribution (in blue) is superimposed on the corresponding model distribution (in pink). The latter is computed for the Sentinel-3 temporal resolution (g) and for the model resolution (h). Sentinel-3 distribution is over 18/06/2016 - 14/03/2019 and the model distribution over

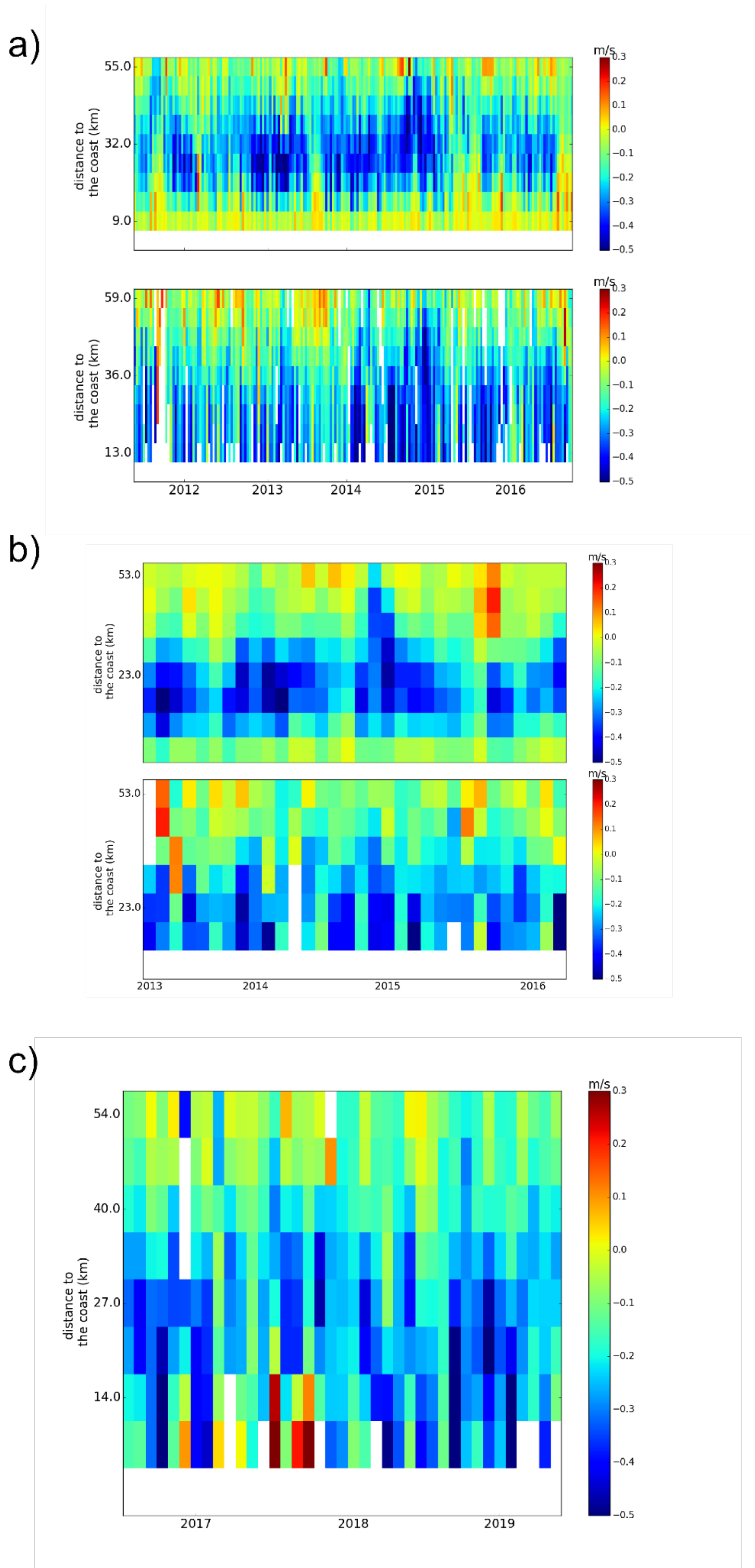

Figure 10: Hovmöller diagrams of the filtered across-track geostrophic current derived along the

altimetry tracks for a) Jason 2 track 222 over 27/05/2011 - 01/10/2016 ; b) SARAL track 302 over 24/03/2013 - 13/03/2016 and c) Sentinel-3 track 472 over 18/06/2016 - 14/03/2019. The corresponding model current is represented at the top panels of a and b.